

1 De novo organelle biogenesis in the cyanobacterium TDX16
2 released from the green alga *Haematococcus pluvialis*

3

4 Qing-lin Dong*, Xiang-ying Xing, Yang Han, Xiao-lin Wei, Shuo, Zhang

5

6 Department of Bioengineering, Hebei University of Technology, Tianjin 300130, China

7 *Correspondence: qldong@hebut.edu.cn

8

9

10

11

12

13

14

15

16

17

18

19

20

21

22

23

24 **Abstract**

25 It is generally accepted that eukaryotic cell arises from prokaryotic cell, which means that organelle can be formed
26 in prokaryotic cell. However, no such an instance has been detected till now. Here, we report organelle biogenesis
27 in the endosymbiotic cyanobacterium TDX16 released from the green alga *Haematococcus pluvialis*, which
28 occurred through six steps. (1) An inner intracytoplasmic membrane (IIM), an outer intracytoplasmic membrane
29 (OIM) and an intervening peptidoglycan-like layer (PL) were synthesized by merging cytoplasmic membrane
30 (CM)-derived thick margin vesicles, which partitioned the thylakoid-less cytoplasm into three compartments: an
31 inner cytoplasm (ICP), an outer cytoplasm (OCP) and a sandwiched intracytoplasmic space (IS). (2) Osmiophilic
32 granules that blistered from CM, OIM and IIM developed into primary thylakoids (PT) in ICP; while OCP
33 disappeared and thus OIM and CM combined into a double-membraned cytoplasmic envelope (CE). (3) ICP
34 decondensed; IIM and PT disassembled into tiny vesicles (TV) and double-membraned vesicles (DMV)
35 respectively. Such that DNA fibers (DF) aggregated and migrated to PL. (4) TV fused into a double-membraned
36 intracytoplasmic envelope (ICE), which re-compartmentalized the coalesced IS and ICP into a new
37 intracytoplasmic space (NS) sequestering most DF and a new inner cytoplasm (NIC) with only few DF. Then
38 ribosomes were formed in both NS and NIC, while DMV opened and extended into secondary thylakoids (ST)
39 only in NIC. (5) NIC developed into the primitive chloroplast (PC) surrounded by ICE, in which ST disassembled,
40 while ST-derived plastoglobuli developed into primitive eukaryotic thylakoids (PMT). After PL dismantled, the
41 matrix of NS was concentrated and encased with the membranes synthesized from ICE-derived dotted vesicles into
42 the primitive nucleus (PN). So, NS vanished, CE wrapped PC and PN. Outside CE, eukaryotic cell wall was
43 formed by assembling sheath at the outer membrane of original cell wall and modifying the peptidoglycan layer. (6)
44 Eukaryotic cytoplasm was built up from the matrix extruded from PN. Mitochondria were assembled in and
45 segregated from PC by encapsulating a portion of stroma with the membranes synthesized from PMT-derived
46 dense-margined vesicles. Then, most mitochondria turned into double-membraned vacuoles after matrix
47 degradation, which mediated unconventional exocytosis and endocytosis. When this process finished, PN got
48 matured into a nucleus enclosed by two sets of envelopes; PC matured into a chloroplast with its PMT maturing
49 into thylakoids. Consequently, the prokaryotic TDX16 cell developed into a eukaryotic cell (TDX16-DE). Results
50 of pigment analysis, 16S rRNA and genome sequencing revealed that TDX16 is a phycocyanin-containing
51 cyanobacterium resembling *Chroococcidiopsis thermalis*, which had acquired 10301 genes from its host, while
52 TDX16-DE is a green alga, whose chloroplast contains chlorophyll b and lutein showing high similarity to that of
53 *Chlorella vulgaris*. Therefore, the mechanism underlying organelle biogenesis in TDX16 was the integration and
54 expression of the obtained genes. Taken together, these results demonstrated that an endosymbiotic prokaryote can
55 develop into a new eukaryote by acquisition and recombination of its eukaryotic host's DNA, which has profound
56 effects on biology, particularly cell and evolutionary biology.

57 **Key words:** De novo organelle biogenesis; endosymbiotic cyanobacterium; *Haematococcus pluvialis*

58 **1. Introduction**

59 All cells are structurally categorized into two groups: eukaryotic cell and prokaryotic cell.
60 Eukaryotic cell contains membrane-bounded compartments called organelles, in which distinct
61 reactions take place. So, organelle biogenesis is essential for cell maintenance and proliferation,
62 which was thought to be achieved only by fission of the preexisting one. Nonetheless, recent
63 studies demonstrated that organelles in the secretory pathway can be formed de novo, including
64 Golgi apparatus (Rossanese et al., 1999; Bevis et al., 2002; Glick 2002; Tängemo et al. 2010;
65 Abiodun and Matsuoka 2013), peroxisomes (South and Gould 1999; Hoepfner et al., 2005; Kim et
66 al., 2006; Rucktäschel et al., 2007; Motley and Hettema 2007; Huber et al., 2012; Opaliński et al.,
67 2012; van der Zand et al., 2012; Sugiura et al., 2017; Hettema and Gould 2017); lysosomes
68 (Kornfeld and Mellman 1989; Blott and Griffiths 2002; Liu et al., 2005; Saftig and Klumperman
69 2009; Luzio et al., 2014; Li et al., 2016; Perera and Zoncu 2016) and vacuoles (Berjak 1972;
70 Marty 1978; Herman et al., 1994; Hoh et al., 1995; Olbrich et al., 2007; Viotti et al., 2013). These
71 results imply that, provided with the information encoded in the genetic material and the
72 machinery needed to interpret this, the cell can produce the organelle with no information in the
73 form of a template or copy of the organelle (Lowe and Barr 2007).

74 In sharp contrast to eukaryotic cell, prokaryotic cell has no organelle. It is widely accepted
75 that eukaryotic cell originates from prokaryotic cell, which means that organelle can be formed in
76 the latter. Paradoxically, however, no instance of organelle biogenesis in prokaryotic cell had been
77 detected. In this case, it has to be assumed that organelle biogenesis in prokaryotic cell occurred
78 only once, during which the first nucleus was formed in an ancient prokaryotic cell, giving rise to
79 the ancestor of eukaryotic cell. Nevertheless, there is another possibility: organelle biogenesis in
80 prokaryotic cell occurred quickly in a short time resulting in the sudden transition of a prokaryotic
81 cell into a eukaryotic cell, and thus was hard to capture.

82 In the previous study we found unexpectedly that the necrotic cells of unicellular green alga
83 *Haematococcus pluvialis* burst and liberated countless small blue cyanobacterial cells (TDX16) in
84 the adverse conditions of high temperature and low irradiance (Dong et al., 2011). TDX16 was
85 light-sensitive, which was relatively stable in the dim light, but turned readily into small green
86 *Chlorella*-like algal cell as light intensity elevated (Dong et al., 2011). The time required for
87 TDX16's transition was short and negatively related to the light intensity, which was about 10
88 days at $60 \mu\text{mol photons m}^{-2} \text{s}^{-1}$. However, light above $60 \mu\text{mol photons m}^{-2} \text{s}^{-1}$ was lethal, causing
89 the disruption of TDX16 cell.

90 TDX16's incredible change was puzzling, which prompted us to investigate if, how and why
91 organelles were formed in its prokaryotic cell. The present study unveiled the biogenesis of

92 chloroplast, nucleus, mitochondrion and vacuole as well as other eukaryotic structures within the
93 thylakoid-less TDX16 cell, owing to the integration and expression of the acquired genes.

94 **2. Results**

95 **2.1 Unusual structure and variable nature of TDX16**

96 Under low light condition, TDX16 cells were always surrounded by thick sheaths (extracellular
97 matrix) and further enclosed within the sporangia (Fig.1-2), showing some similarities to the
98 endospores (baeocytes) of *Chroococidiopsis* (Waterbury and Stanier, 1978; Büdel and Rhiel 1985;
99 Caiola et al., 1993; Caiola et al., 1996; Billi et al., 2000). Most unusually, cells in the same or
100 different sporangia remained at different developmental states with some different inclusions
101 (Fig.1-2). As shown in Fig.1, three different-sized cells (endospores) in a multilayered sporangium
102 were all devoid of thylakoid, but contained one or two membrane-limited heterogenous globular
103 bodies (HGB), and a varied number of cyanobacterial inclusions, including carboxysomes
104 (polyhedral bodies, CX) (Shively et al., 1973; Yeates et al., 2008), polyphosphate bodies (PB)
105 (Allen 1984), osmiophilic granules (lipid globules/bodies, OG) (Lang 1968). HGB contained
106 DNA-like electron-dense granules and filaments and always situated in the nucleoids (NU), where
107 DNA fibers (DF) (Robinow and Kellenberger 1994; Eltsov and Zuber 2006) and ribosomes (RB)
108 (Meene et al., 2006) scattered. The important difference among these cells was that some small
109 swirly and rod-shaped electron-transparent vesicles (EV) were being developed in the left large
110 cell. Similarly, in another five-cells-containing sporangium (Fig.2), the bottom cell contained only
111 OG, while many large different-shaped EV were being formed in the three middle cells, and
112 several thylakoid-like structures were built up in the upper cell.

113 It was evident that EV developed from OG, because (1) OG presented in the small EV, some
114 of them were, however, not in the section plane and thus invisible; (2) as EV enlarged, OG turned
115 into ring-shaped vesicles (RV) after their dense matrixes degraded into to opaque and finally
116 transparent materials (Fig.1-2). OG contained triacylglycerol and tocopherol (Peramuna and
117 Summers 2014), while its exact composition and structure was as yet unknown. There was a
118 general consensus that OG in cyanobacterial cell was comparable to plastoglobuli (PG) in algal
119 and plant chloroplasts (Lang, 1968; Brown and Bisalputra 1969; Findley, 1970; Brđđin et al.,
120 2007), which contained lipids, enzymes, proteins e.g., IM30/ Vipp1 protein (vesicle-inducing
121 protein in plastids 1) and carotenoids, and structurally consisted of a monolayer lipid membrane
122 (half-unit membrane) and a neutral lipid core (Hansmann and Sitte 1982; Smith et al. 2000; Austin
123 et al., 2006; Ytterberg et al., 2006; Vidi et al., 2006; Brđđin and Kessler 2008; Lichtenthaler 2013;
124 Davidi et al., 2015). Nevertheless, the formation of RV in EV indicated that OG had two

125 monolayer lipid membranes, which most likely encased a hydrophilic “protein core”, while the
126 intermembrane space was filled with neutral lipids. So, as the intermembrane space dilated owing
127 to the synthesis of low-density lipids or the like, the outer monolayer membrane bulged and gave
128 rise to an EV; while the interior monolayer membrane and the protein core remained as a
129 monolayer membrane-bounded OG, which subsequently transformed into a RV after the protein
130 core was metabolized or degraded for membrane-remodeling (Fig.1-2).

131 The above results demonstrated that unlike the genuine thylakoid-less cyanobacterium
132 *Gloeobacter violaceus* (Rippka et al., 1974), TDX16 was hypersensitive to light and highly
133 variable in nature, whose anomalous change could not be inhibited completely even in the dim
134 light. Therefore, it was not surprising that when grew in high light regime, TDX16 changed
135 fundamentally in cell structure and pigmentation which were described in the following sections.

136 **2.2 Compartmentalization and biogenesis of primary thylakoids**

137 **2.2.1 Synthesis of intracytoplasmic membranes and peptidoglycan-like layer**

138 Under high light intensity, TDX16 with surrounded sheath escaped from the ruptured sporangium
139 and changed rapidly in structures and inclusions (Fig.3A). PB and CX disappeared, HGB became
140 nearly empty leaving only few DNA-like fibrils and electron-dense margin residues; while a
141 startling number of OG and stacks of membranous elements emerged, and many small EV were
142 being developed (Fig.3A).

143 The most striking change was, however, the compartmentalization of cytoplasm that was
144 enclosed by the cytoplasmic membrane (CM) (Fig.3A). TDX16’s cell wall, like those of other
145 cyanobacteria and gram-negative bacteria (Edwards, et al., 1968; Glauert and Thornley 1969;
146 Hobot, 1984; Beveridge, 1999; Hoiczky and Hansel 2000; Liberton et al., 2006), comprised an
147 outer membrane (OM) and an electron-dense peptidoglycan layer (P), which was separated from
148 CM by an electron-transparent extracytoplasmic (periplasmic) space (ES) (Fig.3A). Inside the
149 cytoplasm, two intracytoplasmic membranes and an intervening peptidoglycan-like layer (PL)
150 were being synthesized, which initiated from a start point and extended parallel to CM (Fig.3A).
151 As a result, the cytoplasm was partitioned into three compartments: (1) the inner cytoplasm (ICP)
152 delimited by the inner intracytoplasmic membrane (IIM), (2) the outer cytoplasm (OCP) of
153 variable thickness bounded by the outer intracytoplasmic membrane (OIM) and CM, and (3) a
154 sandwiched intracytoplasmic space (IS) that was further separated by PL into an outer
155 intracytoplasmic space (OIS) and an inner intracytoplasmic space (IIS) (Fig.3A). It was important
156 that OCP began to reduce or degrade in localized regions near the start point, such that OIM got

157 closed to but not connected with CM (Fig.3A). Compartmentalization also commenced in some
158 cells growing in the low light just as the formation of EV (Fig.1-2). In all these cases, there was no
159 continuity between the intracytoplasmic membranes and CM, and thus the formers were not
160 developed by invagination of the latter. Instead, OIM, IIM and PL were synthesized synchronously
161 by fusion of the small thick margin vesicles (TMV) blistered from the inner leaflet of CM
162 (Fig.3A), which occurred in two probable ways: (1) if TMV were delimited by a half-unit
163 membrane, they first released their contents for synthesizing the septal PL and then fused
164 alternately on its two sides; (2) if TMV were limited by a unit membrane, as they fused one
165 another, the septal PL was synthesized within the coalesced vesicles, a scenario somewhat similar
166 to the formation of cell plate during cytokinesis (Samuels et al., 1995).

167 **2.2.2 Production of OG**

168 Concurrent with compartmentalization, plentiful OG of various sizes blistered from the inner and
169 outer leaflets CM (Fig.3A), such a scenario was also observed in the cells growing under low light
170 condition but the numbers of OG were limited (Fig.1-2). More importantly, some small OG also
171 budded from the inner leaflet of OIM and outer leaflet of IIM (Fig. 3A). These results suggested
172 that the newly formed OIM and IIM were comparable or equivalent to the multifunctional CM, on
173 which both photosynthesis and respiration performed just like the case of the cytoplasmic
174 membrane of *Gloeobacter violaceus* (Rippka et al., 1974; Rexroth et al., 2001), and many
175 metabolites were synthesized as were the cases in the cytoplasmic membranes of all cyanobacteria.
176 These metabolites included (1) peptidoglycan (Egan et al., 2016), phospholipid and lipid
177 intermediates (Osborn et al., 1972); (2) chlorophyll precursors (Peschek et al., 1989) and
178 carotenoid (Bullerjahn and Sherman, 1986); (3) photosystem core complexes (Smith and Howe
179 1993; Zak et al., 2001; Keren et al., 2005) and (4) IM30/ Vipp1 protein (Li et al., 1994; Westphal
180 et al., 2001; Huang et al., 2002; Srivastava et al., 2006) that was proposed to be involved in
181 genesis of thylakoid membranes (Li et al., 1994; Westphal et al., 2001; Aseeva et al., 2007), or
182 assembly of photosystems (Gao and Xu 2009; Zhang et al., 2014).

183 OG was formed by protrusion of the bilayer of CM, OIM and IIM as they were enclosed by
184 two half-unit membranes (Fig.1-2) and apparently played different roles. OG blistered from the
185 inner leaflet of CM, OIM and IIM migrated into ICP for development of EV (Fig.3A); while those
186 shed from the outer leaflet of CM contacted CW, and thus severed as transport conduits or
187 trafficking vehicles channeling or transferring lipids and carotenoids from CM to the CW (Fig.3A),
188 because these compounds were the constituents of OM (Resch and Gibson, 1983; Jürgens and
189 Weckesser 1985; Hoiczuk and Hansel 2000).

190 **2.2.3 Formation of EV and double-membraned cytoplasmic envelope**

191 As OIM, IIM and PL extended (Fig.3B) and ultimately closed up (Fig.3C), the small EV elongated
192 (Fig.3B) and dilated asymmetrically into swirling ones spiraling around NU, and OG began to
193 merge into large ones (Fig.3C). Thereafter HGB disappeared, while new EV were developed
194 within NU and several electron-opaque particles (EOP) were formed (Fig. 3D). In parallel with
195 these changes, the narrow IS (Fig. 3BC) became widened filling with electron-opaque materials
196 (EOM) (Fig. 3D), while OCP disappeared, such that OIM and CM combined into a
197 double-membraned cytoplasmic envelope (CE) (Fig. 3D), which abutted CW owing to the
198 narrowing of ES (Fig.3D). During this process a mass of electron-dense materials were
199 synthesized on CE and transferred to CW for assembling SH, and thus made these structures
200 indistinct (Fig.3D). SH was loosely compacted, made up of flocculent fibrillary materials (FM),
201 microvesicles (MV) and electron-translucent vesicles (ELV) (Fig.3D).

202 **2.2.4 Development of EV into primary thylakoids**

203 The intraluminal RV swelled up into a dilated-ring-shaped vesicle (DRV), whose membrane
204 ultimately met and combined with EV membrane, giving rise to a unit-membrane-bounded
205 combined vesicle (CV); and then CV coalesced into long ones or flattened out into short slender
206 sacs, termed primary thylakoid (PT) (Fig.4A). In this way, EV developed progressively into short
207 PT with opaque matrix, distributing randomly in ICP (Fig.4B). The short PT further extended or
208 merged end-to-end into long PT; while the long coalesced CV flattened out into PT by
209 localized-constriction. And concurrently several cyanophycin granules (CG) (Lang and Fisher
210 1969; Simon 1973) and EOP were formed (Fig. 4C). Finally, the long PT were adjusted to be
211 parallel-arranged, on which the extrinsic phycobilisomes (PCB) (Gantt and Conti 1969) were
212 assembled (Fig.4D). Compared to other cyanobacterial thylakoids, PT exhibited primordial
213 features: thick margin, wide luminal space and spacing (interthylakoidal distances).

214 Accompanying PT biogenesis, a number of ELV shed from OM into SH (Fig.4A), and a mass
215 of DNA fibers were synthesized in ICP (Fig.4D). Occasionally, a group of small RV presented in
216 an EV (Fig.4B), which was probably formed during OG fusion (Fig. 4A) and merged later into
217 large one.

218 **2.3 Re-compartmentalization, DNA translocation and repartition,** 219 **and biogenesis of secondary thylakoids**

220 **2.3.1 Disassembly of PT and IIM, decondensation of ICP and DNA translocation**

221 The newly formed PT promoted TDX16's photosynthetic capacity, but were disassembled soon
222 afterwards. As shown in Fig.5A, PT disassembly initiated with the condensation of luminal matrix,
223 such that PT membrane pair was in closely apposition, seeming to be a single membrane with
224 rough margin. In the meantime, ICP decondensed (solubilized) and became translucent, in which
225 short DF dispersed, some less electron-dense materials (LDM), less electron-dense bodies (LDB)
226 and CG were formed (Fig.5A); IIM disassembled into tiny vesicles (TV), so LDM diffused
227 outward, blurring the compacted PL, CE and CW (Fig. 5A). Subsequently, the solubilized ICP was
228 separated into two portions by LDM: in the lower portion, PT broke up into double-layered
229 membrane fragments (DMF, two unit membranes) and in parallel DF aggregated; while in the
230 upper portion, DMF began to curl and merge laterally into double-membraned vesicles (DMV)
231 (Fig.5B). When all DMF disappeared, a crowd of DMV was formed and numerous DF aggregated
232 (Fig.5C). Thereafter, DMV moved outward quickly and attached to PL that was cover by
233 electron-dense materials, while the intermingled DF scattered outward slowly resulting in an
234 "empty" inner space (EIS), at the border of which the recruited TV began to fuse into
235 double-layered membrane segments (DMS) (Fig. 5D).

236 **2.3.2 Re-compartmentalization, DNA reallocation and formation of secondary** 237 **thylakoids**

238 As DMS coalesced and extended into a double-membraned intracytoplasmic envelope (ICE), the
239 coalesced ICP and IIS was re-compartmentalized into a new inner cytoplasm (NIC) and a new
240 inner intracytoplasmic space (NIS) (Fig.6A). NIC was enclosed by ICE; while NIS represented the
241 space between ICE and PL. Most DF was allocated into NIS, which decondensed into cloudlike
242 materials or aggregated into thick threads; by contrast only few sporadic DF and electron-dense
243 particles (EP) were portioned into NIC (Fig.6A). ICE was not sealed, on the outer leaflet of which,
244 some electron-transparent materials were synthesized (Fig.6A), similar in appearance to the
245 bacterial lipid (Packter and Olukoshi 1995; Alvarez et al., 1996; Kalscheuer et al., 2007).
246 Accompanying ICE expansion, DF in the narrowing NIS decondensed and attached to the
247 thickened PL (Fig.6B); while DMV that were covered by LDM detached from PL, moving inward
248 via ICE opening into NIC or outward through PL pores into OIS (Fig.6B). Therefore, the
249 fenestrated PL served not only as a mechanical and osmotic barrier, but also a platform for
250 anchoring DNA and DMV.

251 When ICE was sealed, DNA in NIS recondensed into thick DF with concomitant formation

252 of countless RB (Fig. 6C). Meanwhile, an increased number of DF and a myriad of RB were also
253 formed in NIC; DMV opened up, retransformed into DMF (Fig. 6C). Thereafter, DMF extended
254 randomly into spiral thylakoids, which was devoid of PCB and morphologically different from PT,
255 termed secondary thylakoids (ST) (Fig.6D). Concomitant with the appearance of ST was the
256 formation of OG and EOB as well as enrichment of DF and RB (Fig.6D). The structures outside of
257 NIC were fuzzy owing to the diffusion of electron-dense materials: the major portion of PL
258 dismantled, such that NIS and OIS coalesced into a new intracytoplasmic space (NS), whose
259 content became the new intracytoplasmic matrix (NX). Aside from DMV, several large
260 electron-translucent oblong vesicles (OV) and electron-opaque vesicles (EOV) emerged in NS
261 (Fig.6D).

262 The viability of the cell indicated that NIC was capable of both photosynthesis and
263 respiration just like a cyanobacterium. So, ST was equipped with photosynthetic and respiratory
264 electron transfer chains as are the cyanobacterial thylakoids (Smith and Howe 1993; Cooley and
265 Vermaas 2001; Lea-Smith et al., 2013; Mullineaux 2014). Whereas, NIC contained only a small
266 amount of DNA, consequentially most of the proteins it required were synthesized in and imported
267 from NX. Thus, NIC played the roles of chloroplast and mitochondrion, while NX served dual
268 functions of nucleus and cytoplasm.

269 **2.4 Biogenesis of primitive chloroplast, eukaryotic cell wall and** 270 **primitive nucleus**

271 **2.4.1 Biogenesis of primitive eukaryotic thylakoids, primitive chloroplast and** 272 **eukaryotic cell wall**

273 Immediately after the emergence of transitional ST, drastic changes occurred in different
274 compartments. As shown in Fig.7A, NIC became polarized, in which ST underwent disassembly,
275 leaving some remnants in the lower region; while parallel arrays of discrete slender sacs with
276 transparent matrix were being developed in the upper region (Fig.7A). These parallel-arranged
277 slender sacs were morphologically similar to algal and plant thylakoids, termed the primitive
278 eukaryotic thylakoids (PMT). Beneath PMT, a nascent pyrenoid (PD) with an incomplete starch
279 plate (SP) and two starch granules (SG) were formed (Fig.7A), both of which were the
280 characteristic bodies of green algal chloroplasts (Gibbs, 1962). So, NIC developed into a primitive
281 chloroplast (PC) delimited by ICE. That was to say, ICE became the chloroplast envelope (CHE).
282 PMT were developed from PG produced during disassembly of ST (Fig.7A), in a way similar but

283 not identical to the biogenesis of PT from OG (Fig.4). The absence of mitochondrion implied that
284 respiration still performed on PMT. Thus, PC was a compound organelle sharing the functions of
285 chloroplast and mitochondrion.

286 NS became widened and clear: NX condensed, containing RB and newly assembled
287 chromatin fibers (CF) (Hay and Revel, 1963; Horowitz et al., 1994); PL and DMV disappeared,
288 while many small dotted vesicles (DV) blistered from CHE and lined up along CE, some of which
289 began to fuse and flattened into membrane segments (MS) (Fig.7A). Such a scenario of membrane
290 synthesis was akin to the assembly of nuclear envelope in vitro or in vivo during open mitosis
291 (Lohka and Masui 1983; Newport, 1987; Vigers and Lohka 1991; Jian et al., 1994). Furthermore, a
292 large coated-vesicle-like opaque-periphery vesicle (OPV) was being assembled at CHE, which
293 appeared to bridge CHE and CE for transferring substances.

294 The fluffy SH (Fig.6D) was organized into a multilayered one, which adhered to OM and
295 made the latter hard to discern (Fig.7A). Such that the new stratified SH and CW seemed to be a
296 continuum (entity), similar in appearance to the cell wall of eukaryotic cell, referred to as the
297 eukaryotic cell wall (EW). The formation of new SH implied that CE and OM were remodeled,
298 while the peptidoglycan layer (P) underlying OM turned into an electron-dense layer (EL). There
299 were a large number of rounded or flattened small vesicles (SV) in the new SH, similar to the
300 vesicles or 'fleck-like' membrane elements in the algal cell wall (Barton 1965; Meindl et al., 1992).
301 Since some smaller vesicles (SMV) budded from the outer leaflet of CE (Fig.7A), it was
302 conceivable that CE incorporated DMV or the like within NS (Fig.6D) for membrane expansion
303 and then gave rise to SMV; in turn SMV were fused into OM, from which SV shed into the new
304 SH.

305 **2.4.2 Encapsulation of the concentrated NX into a primitive nucleus**

306 As PG developed progressively into CV and then flattened into PMT with wide luminal space in
307 the lower PC region, PD got matured, surrounded with a complete SP and bisected by two pairs of
308 PMT. Hence, PC expanded substantially, occupying most NS (Fig.7B). Subsequently, PMT
309 coalesced and extended around PD (Fig.7C). The membranes of adjacent PMT were connected,
310 giving the appearance to be a single membrane. So, PC expanded further and occupied whole NS
311 in the longitudinally sectioned planes; CHE adhered to CE, from the latter of which a dense
312 vesicle (DSV) shed off into the widened ES (Fig.7C). Vertical profile (Fig.7D) showed that the
313 anterior portion of NS disappeared owing to PC expansion, such that NX in the shrunken NS
314 around the posterior portion of PC was concentrated by squeezing out liquid into ES, at the border
315 of which MS coalesced into a limiting membrane (LM) (Fig.7D). As PC expansion continued, NX
316 moved to (Fig. 7E) and finally converged at one side of PC, which was ensheathed by LM and

317 turned into the primitive nucleus (PN) (Fig. 7F). Consequently, LM became PN envelope (PNE),
318 NS vanished, and in turn CE shrank and wrapped PC and PN (Fig. 7F).

319 PN sequestered the concentrated NX containing CF and RB (Fig. 7F) and thus, like PC, was
320 also a compound organelle functioning as nucleus and eukaryotic cytoplasm; while PNE seemed
321 to be consisted of four unit membranes, because it was synthesized by coalescence of DV, which
322 budded from CHE and appeared being bounded by two unite membranes (Fig. 7A). Moreover,
323 EW was osmotic-sensitive, whose outer layer SH shed frequently during cell fixation (Fig. 7 EF).
324 This result confirmed that EW was loosely compacted owing, at least partially, to the insertion of
325 SV and ELV.

326 **2.5 Formation of eukaryotic cytoplasm and biogenesis of** 327 **mitochondrion**

328 **2.5.1 Concurrent formation of eukaryotic cytoplasm and biogenesis of** 329 **mitochondria**

330 As shown in Fig.8A, a vesicle-containing body (VB), apparently derived from the invaginated PC,
331 was being engulfed by PN with concomitant formation of a thin layer of electron-dense materials.
332 PNE was contiguous with CE at the outer side, but separated into two sets of double membraned
333 envelopes inside PC cavity, the inner and outer sets of which were referred to as nuclear envelope
334 (NE) and outer nuclear envelope (OE) respectively. This result confirmed that PNE was consisted
335 of four unit membranes. The thin layer of electron-dense materials was extruded from PN at the
336 site where NE and OE fused, which contained RB and thus was the nascent eukaryotic cytoplasm
337 (EM). Concurrent with the formation of EM, a small mitochondrion (M) was being assembled in
338 PC. After ‘digestion’ of VB, PN and EM both increased in sizes; and an oval mitochondrion with
339 characteristic cristae (CR) emerged in the apical dome of the enlarged PC cavity (Fig.8B). NE and
340 OE were separated by an interenvelope space (IES), but merged at one site resulting in a wide
341 opening, from which nuclear matrix (i.e. EM) was extruded. RB in EM were larger than those
342 within the PC stroma (SM), most of which were attached to the organelles (Fig.8B). During this
343 process, a number of SMV and microfibrils (ML) budded and emanated from CE into ES (Fig.8B).
344 Concurrent nuclear matrix extrusion and mitochondrion formation were observed in different cells
345 (Fig. 8CDE), and two spindle-shaped mitochondria were just being assembled in a PC (Fig. 8D).
346 Occasionally, an intranuclear body (IB) appeared in a PN (Fig.8F), which seemed to be developed
347 during engulfment and digestion of VB or the like, and play a role in selective extrusion of nuclear
348 matrix.

349 **2.5.2 Continuous biogenesis of mitochondria after building up EM**

350 After formation of EM, bulk matrix extrusion from PN ceased, so PN got matured into nucleus
351 (NU); while PC was not the case, in which new mitochondria were developed continuously even
352 after the emergence of vacuoles (V) with internal vesicle (IV), multilamellar body (MLB), lipid
353 droplet (LD), and small opaque vesicle (SOV), leading to the distortion of PMT (Fig.9). As shown
354 in Fig.9A, a small mitochondrion was being developed at the PC edge; while a twisting
355 dumbbell-shaped mitochondrion was nearly finished, one of its bulbous-end sequestering an
356 internal body (ITB) was segregated, but another end was contiguous with PC (Fig.9B). Details of
357 mitochondrion biogenesis were displayed during the assembly of giant mitochondria. As shown in
358 Fig. 9C, a large unfinished 'L-shaped' mitochondrion was continuous with PC in the region
359 around its corner point: the inner side envelope of its long arm and the corresponding portion of
360 CHE, as well as the interior CR were nearly complete; while those of its short arm were just being
361 synthesized. All these membranes were synthesized by merging the small dense-margined vesicles
362 (DGV) developed from the segmented PMT (Fig.9C). Consequentially, mitochondria envelope
363 (ME) and the corresponding portion of CHE were consisted of two unit-membranes; while CR,
364 like PT, ST and PMT, was delimited by a unit-membrane. Similarly, in another cell a bulky
365 mitochondrion was undergoing segregation, which was connected with PC on the inner side but a
366 small mitochondrion on the outer side (Fig.9D). In the inner and outer interfaces, three and two
367 pairs of contorted membranes were being synthesized respectively by fusion of DGV: among the
368 three pairs of membranes, the outer and middle ones were the segments of ME and CHE
369 respectively, while the inner one was likely the envelope of the next mitochondrion that appeared
370 to be in preparation; likewise the two pairs of membranes were the outer side and inner side ME of
371 the bulky and small mitochondria respectively (Fig.9D).

372 The above results demonstrated that mitochondrion was assembled in PC by encapsulating a
373 selected portion of stroma with the membranes derived from PMT. As the assembly was nearly but
374 not completely finished, CHE opened up at the ventral side of PC, allowing the detachment of
375 mitochondrion and then resealed by incorporating CHE segment formed interior to the
376 mitochondrion. Since mitochondria were always assembled in the ventral side of PC where a large
377 nucleoid-like structure (NT) situated (Fig.9D), it was possible that mitochondrial DNA was
378 synthesized in NT and subsequently sorted along with other constituents into mitochondria.

379 **2.6 Biogenesis of vacuoles and degradation of PMT-derived vesicles**

380 **2.6.1 Mitochondria turned into vacuoles after matrix-degradation**

381 Following the emergence of new mitochondrion, the opaque matrix of previously formed
382 mitochondrion began to degrade into transparent material (Fig. 10A), such that the mitochondria
383 turned into double-membrane-bounded vacuoles (V), containing ITB, IV and remnant CR, or only
384 electron-transparent matrix (Fig. 10B). In parallel with vacuole biogenesis, a new mitochondrion
385 was assembled within PC, two LD were developed at CE and a piece of chloroplast debris (CD)
386 emerged in EM (Fig.10B). Hereafter, most ITB decomposed into electron-dense debris (ED)
387 (Fig.10C), which was subsequently expelled outside into EM (Fig. 10D); while some ITB
388 themselves also contained small ITB, so after degradation of their contents, the residual
389 membranes (Fig. 10D) collected into MLB (Fig, 10 EF), resembling those in plant and animal
390 cells (Dermaut et al., 2005; Paquet et al., 2013; Fernandez et al., 2013; Doorn et al; 2015).

391 Degradation of mitochondrial matrix was likely caused by the hydrolases released from CR;
392 while the enzymes for ITB decomposition were presumably liberated from the space between its
393 two limiting membranes, similar to the cases proposed for the transition of provacuole or
394 autophagosome into vacuoles (Buvat and Robert, 1979; Marty 1999; Doorn and Papini, 2013) and
395 double-membrane-bounded vacuoles (Aubert et al., 1996) in plant cells. Moreover, it was
396 noteworthy that several cobblestone-shaped DRV appeared in EV (Fig.10F), confirming that PMT
397 in PC was developed in a way similar to that of PT.

398 **2.6.2 Formation and degradation of PMT-derived vesicles and coalescence of** 399 **vacuoles**

400 After vacuoles came into being, some short PMT in PC curled and ‘rolled up’ into “vesicle within
401 vesicle” like compound vesicles (CPV) (Fig.11 ABC), which were taken up by vacuoles directly
402 as they got segregated from PC (Fig. 11C), or after they shed into EM (Fig.11AB). After the
403 internalized CPV released their contents for degradation, the remaining membranes stacked up
404 into MLB (Fig. 11DEF). The vacuoles fused with each other by membrane protrusion. As shown
405 in Fig. 11CD, a vacuole protruded into another one and fused at the contact sites, such that the
406 membrane protrusion pinched off and became an IV (Fig.11E) or shed as MF (Fig. 11DF). When
407 PC dwindled to a normal size, no more mitochondria and CPV were produced and all vacuoles
408 coalesced into a large single one (Fig.11F). Hence, PC got matured into chloroplast (C) and as
409 such PMT matured into eukaryotic thylakoids (T).

410 During vacuole biogenesis, cluster of SOV and tubules (TE) resembling the internal vesicle
411 (body) of multivesicular body (Harding et al., 1983; Pan et al., 1985) was developed most likely
412 from CD (Fig. 10B; Fig.11E) in the vicinity of nucleus or vacuoles (Fig.9C; Fig.11CDEF). CD

413 and VB (Fig.8A) were excised directly from PC, the latter of which was engulfed by PN. So, the
414 content of CD was probably degraded by the enzymes released from nucleus, while the remaining
415 PMT fragments coiled into SOV, part of which were internalized by vacuole and became IV
416 (Fig.9D).

417 **2.7 Vacuole mediated unconventional exocytosis and endocytosis**

418 **2.7.1 Vacuole-mediated unconventional exocytosis**

419 Vacuoles came into contact and fused with CE, and then the fused membranes broke up into
420 fragments resulting in large openings, from which a small quantity (Fig. 10DF; 12A) or a large
421 amount of vacuolar content and SOV (Fig.12B) were expelled into ES. These expelled SOV were
422 internalized from the neighboring SOV clusters (Fig.12B), which acted as exosomes (Johnstone et
423 al., 1987; Théry et al., 2002) and perhaps transferred specific cargos to OM. Undoubtedly, the
424 exocytotic materials contained proteins for remodeling the surface of CE and OM as well as
425 thickening EW, which were sourced from PC, but not synthesized on endoplasmic reticulum (ER)
426 and sorted through Golgi apparatus (GA) as did the normal secreted proteins (Rothman and
427 Wieland, 1996; Schekman and Orci, 1996; Schatz and Dobberstein 1996). Therefore, the
428 vacuole-mediated exocytosis was an unconventional (nonclassical) route of protein secretion
429 (Nickel and Rabouille 2009; Zhang and Schekman, 2013; Ding et al., 2014; Robinson et al., 2016;
430 Rabouille 2017). During exocytosis, the vacuolar membranes were apparently in vast excess of
431 that required for cell expansion (Fig. 10DF; Fig.12AB), so the vacuole-mediated unconventional
432 exocytosis released only a portion of the vacuolar content each time, more or less similar to the
433 transient-fusion exocytosis (De Toledo et al., 1993) and open and closed exocytosis (Ren et al.,
434 2016).

435 **2.7.2 Vacuole-mediated unconventional endocytosis**

436 The double-membranes of vacuole merged with CE at two distant sites and then invaginated,
437 resulting in a large invaginated space (IVS), entrapping some electron-dense fibrils (EF) and
438 globular particles (GP); while CE between the two merged sites disrupted and coiled into
439 membranous structures (Fig.12C). Upon IVS reaching certain size, the membrane invagination
440 pinched off into the vacuole lumen and became a large IV, whose content was degraded in situ or
441 discharged into the vacuole lumen (Fig.12D). In the same way, the nascent vacuole also mediated
442 small episode of endocytosis (Fig.10C). Evidently, the vacuole-mediated endocytosis was an
443 unconventional endocytic route and distinct from the conventional endocytosis, where the small

444 endocytic vesicles passed their contents successively through the early endosome (trans-Golgi
445 network) and late endosome (multivesicular body or pre-vacuolar compartments) for protein
446 sorting and finally to the vacuole or lysosome for degradation (Blott and Griffiths 2002; Mayor
447 and Pagano 2007; Saftig and Klumperman 2009; McMahon and Boucrot 2011; Chen et al., 2011;
448 Fan et al., 2015). During this unconventional endocytic process, the vacuolar membranes were
449 insufficient for IV development. Given that MLB presented in the vacuole with small invagination
450 (Fig. 9D), but disappeared in the vacuole with large invagination Fig. 12C), it was possible that
451 MLB served as membrane source for developing large IV.

452 **2.8 Structure and reproduction of the TDX16-derived eukaryotic cell**

453 **2.8.1 Structure of the TDX16-derived eukaryotic cell**

454 After bulk exocytosis and endocytosis, the large vacuoles disappeared, while the distorted
455 thylakoids in the chloroplast straightened with narrowed luminal spaces (Fig.13ABC). As a result,
456 the prokaryotic TDX16 cell (Fig.1-2) developed eventually into a stable eukaryotic cell with
457 unique structure (Fig.13ABC). The TDX16-derived eukaryotic cell (TDX16-DE cell) was
458 surrounded by an OM-containing EW, an ES of variable widths and a double-membraned CE,
459 containing a characteristic “e-shaped” chloroplast, a nucleus with OE and NE, usually two
460 mitochondria and frequently two or more small double-membrane-bounded vacuoles, but no EM,
461 GA and peroxisomes (Fig.13ABC). Hence, OE, NE and CE served dual or multiple functions;
462 while OM and ES consistently played similar roles as they did before organelle biogenesis (Fig.
463 1-6), though their composition and content apparently changed.

464 The large nucleus with no visible pores on OE and NE still contained a few RB (Fig.13ABC).
465 When OE and NE became widely separated, some electron-dense vesicles (EDV) budded from
466 NE into IES, and then fused with and re-budded from OE, ultimately migrated to the inner leaflet
467 of CHE as well as the inner and outer leaflets of CE (Fig.13B), which probably delivered
468 nucleus-synthesized and or imported proteins for maintaining the corresponding envelope
469 membranes. If so, the transportation of nucleus-synthesized and or imported proteins into ES with
470 NE-derived vesicles was another way of unconventional exocytosis. During this process OE
471 disrupted locally resulting in several openings, and more importantly, an opening was also formed
472 at the contact site of OE and CE. Such that the proteins synthesized in EM could be sorted through
473 OE openings into IES and then secreted via the opening on CE into ES (Fig. 13B). By contrast,
474 when OE and NE came into contact, they fused at several sites and thus gave rise to openings,
475 allowing nucleocytoplasmic transport (Fig.13C). Amazingly, a fusion pore was formed at the

476 contact site of NE, OE and CE (Fig.13C), enabling the direct communication between nucleus and
477 ES.

478 CE was the major site of lipid synthesis. As shown in (Fig.13C), three large and one nascent
479 LD were assembled at CE inner membrane. Similar cases were frequently observed since the
480 degradation of mitochondrion (Fig. 9BCD; Fig.10 BCDF; Fig.11 DEF; Fig.12AB). By contrast,
481 LD was only occasionally formed at CHE (Fig.10C). Since OG was initially blistered from the CE
482 outer membrane (CM), CE inner membrane (OIM) and IIM (Fig.1-3), these results demonstrated
483 that CE was consistently the site of lipid synthesis; while OIM-derived CHE was also capable of
484 lipid synthesis. Accordingly, EOV formed earlier were probably the primordial LD (Fig.6D;
485 Fig.7ABF; Fig. 8CDF). In addition, EOB in NIC (Fig. 6D) and PC (Fig.7ABC; Fig.8D; Fig.12B)
486 were perhaps analogous to LD, which seemed to be developed at PT and ST, similar to LD
487 formation in the green alga (Fan et al., 2011; Goodson et al., 2011). So, EOB were likely packed
488 into ITB of mitochondria and CPV, and subsequently expelled into EM in the form of LD
489 (Fig.10E; Fig.11E).

490 EW, as described above (Fig. 7A), was consisted of a SH, an EL and an intervening OM
491 (Fig.13B). Hence, ES was a membrane-surrounded compartment but not the extracellular space,
492 which sequestered the liquid squeezing out from NX and likely served important functions in cell
493 metabolism (Fig.7). Since ELV blistered consistently from OM into SH before (Fig.3-6), during
494 (Fig.7-12) and after (Fig.13) organelle biogenesis, it was nearly certain that OM in EW was still
495 the enzyme-anchoring site and responsible for assembling and modifying the external SH (Fig.3A).
496 EL was likely perforated just as the original peptidoglycan layer (Fig.3A) allowing the passage
497 and fusion of SOV and the like with OM.

498 **2.8.2 Reproduction of TDX16-DE cell**

499 TDX16-DE cell multiplied via autospore. As shown in Fig.13D, four autospores within an
500 autosporangium (AUG) were segregated from each other by the wide interspace, more or less
501 similar to the arrangement of TDX16 (endospores) in the sporangium (Fig.1). All these autospores
502 contained a chloroplast of various sizes. In addition, the smallest autospore possessed a large
503 nucleus, while the two large ones had mitochondrion and vacuoles and the last one had no other
504 organelle at all. Hence, nucleus, mitochondrion and vacuole in most endospores were not allocated
505 from the mother cell but developed from scratch. The constant presence of chloroplast but absence
506 of mitochondrion in some TDX16-DE cell suggested that the chloroplast thylakoids still retained
507 respiratory electron transfer chains and were capable of oxidative phosphorylation, i.e.,
508 chlororespiration (Bennoun 1982; Peltier and Courmac 2002).

509 **2.9 Photosynthetic pigments of TDX16 and TDX16-DE cell**

510 In vivo absorption spectra (Fig.14A) showed that apart from the absorption maxima of chlorophyll
511 a (Chl a) at 440 and 680 nm, TDX16 displayed a prominent peak at 630nm, corresponding to
512 phycocyanin (PC) (Lemasson et al., 1973); while TDX16-DE cell exhibited a conspicuous
513 shoulder peak of chlorophyll b (Chl b) at 653 nm (Govindjee and Rabinowitch, 1960), and a
514 merged peak of carotenoids around 485 nm. Consistent with these results, fluorescence emission
515 spectroscopy indicated that the water soluble pigment extract of TDX16 (Fig. 14E) and lipid
516 soluble pigment extract of TDX16-DE (Fig. 14F) displayed an emission peak of PC at 646 nm
517 (Gantt et al., 1979) and an emission peak of Chl b at 658 nm (Thorne et al., 1977) respectively, but
518 no emission peak was detected in the water soluble pigment extract of TDX16-DE (Fig. 14E) and
519 lipid soluble pigment extract of TDX16 (Fig. 14F). Furthermore, PC isolated from TDX16 had an
520 absorption peak at 617nm (Fig. 14B), nearly the same as C-PC (Gantt et al., 1979); Chl b and
521 lutein separating from TDX16-DE cell displayed absorption maxima at 456 and 645 nm (Fig.
522 14C), 420, 446 and 475nm (Fig. 14D) respectively, identical to those isolated from plants
523 (Lichtenthaler, 1987).

524 **2.10 16S rRNA sequences of TDX16 and TDX16-DE cell**

525 16S rRNA of TDX16 (GenBank KJ599678.2) and TDX16-DE chloroplast (GenBank KJ612008.1)
526 shared a low identity of 83%, but showed high similarities of 98% and 99% to that of
527 *Chroococidiopsis thermalis* (GenBank NR102464.1) and those of the chloroplasts of
528 *Auxenochlorella protothecoides* (GenBank AY553213.1) and *Chlorella vulgaris* (GenBank
529 AB001684.1) respectively.

530 **2.11 Genome sequence of TDX16**

531 TDX16 genome was 15,333,193 bp in size with an average of GC content of 55.2 % containing
532 15,894 genes (CDS 15,756; RNA 138). This Whole Genome Shotgun project has been deposited
533 at DDBJ/ENA/GenBank under the accession NDGV00000000. The version described in this
534 paper is version NDGV01000000.

535 **3. Discussion**

536 The present study unveiled the biogenesis of chloroplast, nucleus, mitochondrion and vacuoles
537 within the prokaryotic cell of TDX16. Consequentially, an essential question arose as to why this

538 happened? Or what was the reason for organelle biogenesis in TDX16 cell?

539 The consistent results of cell structure (Fig.1-2), pigmentation (Fig.14) and 16S rRNA gene
540 sequence indicated that TDX16 was a PC-containing cyanobacterium resembling *C. thermalis*.
541 However the genome size, gene number and GC content of TDX16 (GenBank NDGV00000000)
542 were 2.4, 2.8 and 1.2 times those of *C. thermalis* (6,315,792 bp, 5593 genes and 44.4% GC)
543 (GenBank CP003597.1) respectively. Since TDX16 was an endosymbiotic cyanobacterium
544 released from the necrotic cell of green alga *H. pluvialis* (Dong et al., 2011), these results
545 demonstrated that TDX16 had acquired at least 9,017,401bp DNA with 10301 genes from its host.
546 Therefore, the reason for organelle biogenesis within TDX16 was the light-driven recombination
547 (hybridization) and expression of the obtained eukaryotic genes and its own prokaryotic genes, the
548 process of which was indicated by the changes of cell structures.

549 The obtained DNA was retained most likely in HGB, which contained DNA-like materials,
550 situated in NU and remained a constant size in different cells (Fig.1). When compartmentalization
551 commenced, the obtained DNA was released gradually from HGB into the NU (Fig. 3), most of
552 which kept inactive because the initially formed PT were cyanobacterial ones, owing apparently to
553 the expression of TDX16's own genes that were inhibited within the host cell (Fig.4). During the
554 crucial re-compartmentalization, the total DNA in the solubilized ICP was gathered (Fig.5) and
555 subsequently allocated into NS (major portion) and NIC (minor portion), where the obtained DNA
556 and TDX16's own DNA began to recombine as indicated by the dismantling of PL and absence of
557 PCB on the transitional PT-derived ST (Fig. 6). DNA-recombination quickly finished leading to
558 the formation of PC sequestering the genes of chloroplast and mitochondrion and PN containing
559 nucleus genes only (Fig.7). Thereafter, mitochondrial genome was assembled in PC and packed
560 into mitochondria, while the remaining genes were organized into chloroplast genome (Fig. 8-11).
561 So, it was not surprising that mitochondrial and chloroplast genomes shared similar features, and
562 chloroplast genome retained some mitochondrion-related genes. The disappearance of PC (Fig.
563 14), PL (Fig. 7) and TDX16 16S rRNA, but appearance of 16S rRNA of TDX16-DE chloroplast
564 indicated that DNA recombination involved the loss of some prokaryotic genes, but the synthesis
565 new genes. Furthermore, the repartition of total DNA during re-compartmentalization (Fig. 6)
566 inevitably resulted in the distribution of prokaryotic genes in nucleus genome and eukaryotic
567 genes in chloroplast and mitochondrial genomes, giving the appearance of "inter-organellar gene
568 or DNA transfer". On the other hand, TDX16 genes in TDX16-DE cell seemed to be resulted from
569 "prokaryote-to-eukaryote gene transfer".

570 Aside from organelle biogenesis, some long-standing questions in cell biology had been

571 resolved the present study: (1) OG and PG were the precursors of thylakoids in cyanobacteria and
572 chloroplasts respectively; (2) Mitochondrial cristae, like thylakoids in cyanobacteria and
573 chloroplasts, were not formed by invagination of the inner envelope membrane (3) MLB were
574 developed from mitochondrion and chloroplast;(4)Vacuoles and nucleus-derived vesicles mediated
575 unconventional exocytosis; (5) EW contained an OM, and thus ES was a membrane-surrounded
576 compartment; (6) LD were formed predominantly at CE but marginally at CHE. Last but not the
577 least, organelle biogenesis in cyanobacterium TDX16 gave rise to a new green alga (TDX16-DE),
578 which was the first instance of new species formation and demonstrated that a prokaryote can
579 acquire its eukaryotic host's genes and developed into a new eukaryote. Therefore, the discovery
580 of organelle biogenesis in TDX16 is of great importance and has profound effects on cell biology
581 and evolutionary biology.

582 **4. Materials and methods**

583 **4.1 Strain and culture**

584 TDX16 was obtained from the necrotic and ruptured *H. pluvialis* cell (Dong et al., 2011) and
585 maintained under low light intensity of $12 \mu\text{mol photons m}^{-2} \text{s}^{-1}$, at $25 \text{ }^\circ\text{C}$ in the illumination
586 incubator. For experiment, TDX16 was inoculated into sterilized 250-ml Erlenmeyer flasks
587 containing 100 ml BG-11 medium (Stanier et al., 1971) and incubated under high light intensity of
588 $60 \mu\text{mol photons m}^{-2} \text{s}^{-1}$, at $25 \text{ }^\circ\text{C}$.

589 **4.1 Microscopy preparations and observations**

590 Cells were fixed with 2.5% glutaraldehyde and 1% osmium tetroxide, followed by dehydration
591 with ascending concentrations of ethanol, and post staining with 3% uranyl acetate and lead citrate.
592 The samples were examined with a JEM1010 electron microscope (JEOL, Japan).

593 **4.2 Pigment analyses**

594 **4.2.1 In vivo absorption spectra**

595 Cell suspensions were scanned with Ultraviolet-Visible Spectrophotometer Cary 300 (Agilent,
596 USA), the spectra were normalized to give an equal absorbance of Chl a at 440 nm.

597 **4.2.2 Fluorescence emission spectra**

598 Water soluble pigments were extracted with 0.75M K-phosphate buffer (pH=6.8). Lipid soluble

599 pigments were extracted with pure acetone and diluted 50-fold into ethanol. Both extracts were
600 analyzed directly on Fluorescence Spectrophotometer F-4500 (Hitachi, Japan) at room
601 temperature with excitations of 580 and 478 nm respectively.

602 **4.2.3 Pigment separation and identification**

603 Chl b was separated by thin-layer chromatography according to the method described by
604 Lichtenthaler (Lichtenthaler, 1987). PC was extracted and purified following the procedures
605 described by Adams (Adams et al., 1979). All pigments were analyzed with Ultraviolet-Visible
606 Spectrophotometer Cary 300 (Agilent, USA), and identified by spectroscopic matching with the
607 published data.

608 **4.3 16S rRNA sequence**

609 DNA samples were prepared according to the method described previously (Garcia-Pichel et al.,
610 1998). 16S rRNAs were amplified using the primers 8-27f (AGAGTTTGATCCTGGCTCAG) and
611 1504-1486r (CTTGTTACGACTTCACCCC) (Moore et al., 1998). Fragments were cloned into the
612 pMD18-T vector and amplified using M13 forward and reverse universal primers. The PCR
613 products were digested with restriction enzymes BamH1/SalI, and sequenced on ABI 3730 DNA
614 analyzer (PerkinElmer Biosystems, USA).

615 **4.4 Genome sequence of TDX16**

616 TDX16 cells were harvested by centrifugation at 3000 rpm for 10 min, and washed twice with 5M
617 NaCl solution and sterile water alternately, with the pelleted cells being frozen in liquid nitrogen
618 and then grinded with sterile glass beads (0.5 mm diameter).The slurry was transferred into 5ml
619 centrifuge tube with TE buffer (1mM EDTA, 10 mM Tris-HCl, pH=8.0), supplemented with 1.0
620 ml lysozyme solution (20 mg/ml) and incubated at 37 °C for 60 min, then added CTAB
621 (Cetyltrimethyl ammonium bromide) solution (10% CTAB, 0.7 M NaCl) and heated to 65 °C for
622 30 min in a waterbath. After centrifugation (12000 rpm, 10min), the supernatant was extracted
623 with one volume of phenol-chloroform-isoamyl alcohol (25:24:1, V/V), and DNA was precipitated
624 overnight at -20 °C after the addition of 2/3 volume of cold isopropanol and 1/10 volume of 3M
625 sodium acetate, dried and resuspended in TE buffer. The extracted DNA was first subjected to
626 quality assay and then sheared ultrasonically into fragments, with their overhangs being converted
627 into blunt ends applying T4 DNA polymerase, Klenow Fragment and T4 Polynucleotide Kinase.
628 Subsequently, adapters were ligated to the 3' ends of DNA fragments that were introduced with 'A'
629 bases. The obtained fragments were purified via gel-electrophoresis and PCR-amplified for
630 preparing the sequencing library of DNA clusters. Paired-end sequencing was carried out on an

631 Illumina HiSeq 4000 platform, yielding 1.132 Mb raw data. After removal of the low quality reads,
632 1.009 Mb clean data was assembled with SOAPdenovo.

633 **References**

- 634 Abiodun, M.O and Matsuoka, K (2013) Evidence that proliferation of Golgi apparatus depends on
635 both de novo generation from the endoplasmic reticulum and formation from pre-existing
636 stacks during the growth of tobacco BY-2 cells. *Plant Cell Physiol.* 54: 541-554
- 637 Adams, S.M., Kao, O.W and Berns, D.S (1979) Psychrophile C-Phycocyanin. *Plant Physiol.* 64:
638 525–527.
- 639 Allen, M. M (1984) Cyanobacterial cell inclusions. *Annu. Rev. Microbiol.* 38:1-25.
- 640 Alvarez, H. M., Mayer, F., Fabritius, D., and Steinbüchel, A (1996) Formation of intracytoplasmic
641 lipid inclusions by *Rhodococcus opacus* strain PD630. *Arch. Microbiol.* 165:377–386
- 642 Aseeva, E., Ossenbuhl, F., Sippel, C., et al. (2007) Vipp1 is required for basic thylakoid
643 membrane formation but not for the assembly of thylakoid protein complexes. *Plant*
644 *Physiol. Biochem.* 45: 119–128
- 645 Aubert, S., Gout, E., Bligny, R., Marty-Mazars, D., Barrieu, F., Alabouvette, J., Marty, F. and
646 Douce, R (1996) Ultrastructural and biochemical characterization of autophagy in higher
647 plant cells subjected to carbon deprivation: control by the supply of mitochondria with
648 respiratory substrates. *J. Cell Biol.* 133: 1251–1263
- 649 Austin, J.R., Frost, E., Vidi, P.A., Kessler, F., and Staehelin, L.A (2006) Plastoglobules are
650 lipoprotein subcompartments of the chloroplast that are permanently coupled to thylakoid
651 membranes and contain biosynthetic enzymes. *Plant Cell* 18: 1693–1703
- 652 Barton, R (1965) Electron microscope studies on surface activity in cells of *Chara vulgaris*. *Planta*
653 66, 95—105
- 654 Berjak, P (1972) Lysosomal compartmentation: Ultrastructural aspects of the origin, development,
655 and function of vacuoles in root cells of *Lepidium sativum*. *Ann. Bot. (Lond.)* 36: 73–81.
- 656 Bennoun P (1982) Evidence for a respiratory chain in the chloroplast. *Proc. Natl. Acad. Sci. USA*
657 79: 4352–4356
- 658 Beveridge, T. J (1999) Structure of Gram-negative cell walls and their derived membrane vesicles.
659 *J. Bacteriol.* 181: 4725-4733
- 660 Bevis, B. J., Hammond, A. T., Reinke, C. A., and Glick, B. S (2002) De novo formation of
661 transitional ER sites and Golgi structures in *Pichia pastoris*. *Nature Cell Biol.* 4, 750–756
- 662 Billi, D., Friedmann, E. I., Hofer, K.G., Caiola, M.G and Friedmann, R.O(2000) Ionizing-radiation
663 resistance in the desiccation-tolerant cyanobacterium *Chroococcidiopsis*. *Appl. Environ.*

- 664 Microbiol. 66:1489–1492
- 665 Blott, E. J. and Griffiths, G. M (2002) Secretory and lysosomes. Nat. Rev. Mol. Cell Biol.
666 3:122–131.
- 667 Brđđin, C., Kessler, F and van Wijk, K. J (2007) Plastoglobules: versatile lipoprotein particles in
668 plastids. Trends plant sci. 12 (6):260-266
- 669 Brđđin, C and Kessler, F (2008) The plastoglobule: a bag full of lipid biochemistry tricks.
670 Photochem. Photobiol. 84:1388–1394
- 671 Brown, D. L and Bisalputra, T (1969) Fine structure of the blue-green alga *Nostoc sphaericum*: the
672 structured granule. Phycologia 8:119-126
- 673 Büdel, B and Rhiel, E (1985) A new cell wall structure in a symbiotic and free-living strain of the
674 blue-green alga genus *Chroococidiopsis* (Pleurocapsales). Arch. Microbiol. 143: 117-121.
- 675 Bullejtahn, G. S and Sherman, L. A (1986) Identification of a Carotenoid-Binding Protein in the
676 Cytoplasmic Membrane from the Heterotrophic Cyanobacterium *Synechocystis* sp. Strain
677 PCC6714. J. Bacteriol. 167: 396-399
- 678 Buvat, R and Robert, G (1979) Vacuole formation in the actively growing root meristem of barley
679 (*Hordeum sativum*). Am. J. Bot. 66:1219-1237
- 680 Caiola, M. G., Friedmann, R. C and Friedmann, E.I (1993) Cytology of long-term desiccation in
681 the desert cyanobacterium *Chroococidiopsis* (Chroococcales). Phycologia 32: 315-322.
- 682 Caiola, M.G., Billi, D and Friedmann, E. I (1996) Effect of desiccation on envelopes of the
683 cyanobacterium *Chroococidiopsis* sp. (Chroococcales). Eur. J. Phycol. 31:97–105.
- 684 Chen, X., Irani, N.G and Friml, J (2011) Clathrin-mediated endocytosis: the gateway into plant
685 cells. Curr. Opin. Plant Biol. 14: 674–682
- 686 Cooley, J. W., and Vermaas, W. F. J (2001) Succinate dehydrogenase and other respiratory
687 pathways in thylakoid membranes of *Synechocystis* sp. strain PCC 6803: capacity
688 comparisons and physiological function. J. Bacteriol. 183: 4251–4258
- 689 Davidi, L., Levin, Y., Ben-Dor, S and Pick, U (2015) Proteome analysis of cytoplasmatic and
690 plastidic b-carotene lipid droplets in *Dunaliella bardawil*. Plant Physiol. 167: 60–79
- 691 Dermaut, B., Norga, K.K., Kania, A., Verstreken, P., Pan, H. L., Zhou, Y., Callaerts, P and Bellen,
692 H (2005) Aberrant lysosomal carbohydrate storage accompanies endocytic defects and
693 neurodegeneration in *Drosophila benchwarmer*. J. Cell Biol. 170:127–139.
- 694 De Toledo, G. A., Fernandez-Chacon, R and Fernandez, J. M. (1993). Release of secretory
695 products during transient vesicle fusion. Nature 363: 554–558.
- 696 Ding, Y., Wang, J., Wang, J.Q., Stierhof, Y. D., Robinson, D. G., and Jiang, L. W (2012)
697 Unconventional protein secretion. Trends Plant Sci. 17:606-615.

- 698 Dong, Q. L., Li, Z.W., Xing, X.Y., Chen, B (2011) Discovery of an endophytic cyanobacterium in
699 *Haematococcus pluvialis*. J. Hebei Univ. Technol. 40: 1-5
- 700 Edwards, M. R., Berns, D. S., Ghiorse, W.C., and Holt, S. C (1968) Ultrastructure of thermophilic
701 blue green alga *Synechococcus lividus* Copeland. J Phycol 4:283–298
- 702 Egan, A.J., Cleverley, R.M., Peters, K., Lewis, R.J., and Vollmer, W. (2016) Regulation of
703 bacterial cell wall growth. FEBS J. 284: 851-867
- 704 Eltsov, M., and Zuber, B (2006) Transmission electron microscopy of the bacterial nucleoid. J.
705 Struct. Biol. 156:246–54
- 706 Fan, J., Andre, C., and Xu, C (2011) A chloroplast pathway for the de novo biosynthesis of
707 triacylglycerol in *Chlamydomonas reinhardtii*. FEBS Lett. 585:1985-1991.
- 708 Fan, L., Li, R., Pan, J., Ding, Z., and Lin, J (2015) Endocytosis and its regulation in plants. Trends
709 Plant Sci. 20: 388-397
- 710 Fernández, M. C., Pérez-Gutierrez, M. A., Suarez-Santiago, V. N., Salinas-Bonillo, M. J.,
711 Romero-García, A. T (2013) Multilamellar bodies linked to two active plasmalemma
712 regions in the pollen grains of *Sarcocapnos pulcherrima*. Biol. Plant. 57: 298-304.
- 713 Findley, D. L., Walne, P .L., and Holton, R.W (1970) The effects of light intensity on the
714 ultrastructure of *Chlorogloea fritschii* mitra grown at high temperature. J. Phycol. 6:
715 182-188
- 716 Gantt, E., and Conti, S. F (1969) Ultrastructure of blue-green algae. J. Bacteriol. 97: 1486-1493
- 717 Gantt, E., Lipschultz, C. A., Grabowski, J., and Zimmerman, B .K. (1979) Phycobilisomes from
718 blue-green and red algae: isolation criteria and dissociation characteristics. Plant Physiol.
719 63: 615–620.
- 720 Gao, H., and Xu, X (2009) Depletion of Vipp1 in *Synechocystis* sp. PCC 6803 affects
721 photosynthetic activity before the loss of thylakoid membranes. FEMS Microbiol. Lett.
722 292: 63–70.
- 723 Garcia-Pichel, F., Nübel, U., and Muyzer, G (1998) The phylogeny of unicellular, extremely
724 halotolerant cyanobacteria. Arch. Microbiol. 169, 469–482.
- 725 Gibbs, S.P (1962) The ultrastructure of the pyrenoids of green algae. J. Ultra. Res. 7:
726 262-272.
- 727 Glauert, A.M and Thornley M.J (1969) The topography of the bacterial cell wall. Annu. Rev.
728 Microbiol. 23: 159–198.
- 729 Glick, B.S (2002) Can the Golgi form de novo? Nat. Rev. Mol. Cell Biol. 3:615–619.
- 730 Goodson, C., Roth, R., Wang, Z. T., Goodenough, U (2011) Structural correlates of cytoplasmic
731 and chloroplast lipid body synthesis in *Chlamydomonas reinhardtii* and stimulation of lipid

- 732 body production with acetate boost. Eukaryot. Cell 10:1592-1606.
- 733 Govindjee, and Rabinowitch, E (1960) Two forms of chlorophyll a in vivo with distinct
734 photochemical functions. Science 132: 355-356.
- 735 Hansmann, P., and Sitte, P (1982) Composition and molecular structure of chromoplast globules of
736 *Viola tricolor*. Plant Cell Rep. 1 : 111-114
- 737 Hay, E. D., and J. P. Revel (1963) The fine structure of the DNP component of the nucleus. J. Cell
738 Biol. 16:29-51
- 739 Harding, C., Heuser, J., and Stahl, P (1983) Receptor-mediated endocytosis of transferrin and
740 recycling of the transferrin receptor in rat reticulocytes. J. Cell Biol. 97:329–339.
- 741 Herman, E.M., Li, X., Su, R.T., Larsen, P., Hsu, H., and Sze, H (1994) Vacuolar-type H⁺-ATPases
742 are associated with the endoplasmic reticulum and provacuoles of root tip cells. Plant
743 Physiol. 106: 1313–1324.
- 744 Hettema, E.H., and Gould, S. J (2017) Organelle formation from scratch. Nature, 542: 174-175
- 745 Hoepfner, D., Schildknecht, D., Braakman, I., Philippsen, P., and Tabak, H.F (2005) Contribution of
746 the endoplasmic reticulum to peroxisome formation. Cell 122:85–95.
- 747 Hobot, J. A., Carlea, E., Villiger, W., and Kegenberger, E (1984) Periplasmic gel: new concept
748 resulting from the reinvestigation of bacterial cell envelope ultrastructure by new methods.
749 J. Bacteriol. 160:143-152.
- 750 Hoh, B., Hinz, G., Jeong, B. K., and Robinson, D.G (1995) Protein storage vacuoles form de novo
751 during pea cotyledon development. J. Cell Sci. 108, 299-310
- 752 Hoiczkyk, E., and Hansel, A (2000) Cyanobacterial cell walls: news from an unusual prokaryotic
753 envelope. J. Bacteriol. 182: 1191-1199
- 754 Horowitz, R. A., Agard, D. A., Sedat, J. W., and Woodcock, C. L (1994) The three-dimensional
755 architecture of chromatin in situ: Electron tomography reveals fibers composed of a
756 continuously variable zig-zag nucleosomal ribbon. J. Cell Biol. 125:1–10
- 757 Huber, A., Koch, J., Kragler, F., Brocard, C., and Hartig, A (2012) A subtle interplay between three
758 Pex11 proteins shapes de novo formation and fission of peroxisomes. Traffic 13: 157–167.
- 759 Huang, F., Perry, I., Nilsson, F., Parson, A. L., Pakrasi, H. B., Andersson, B., and Norling B (2002)
760 Proteomics of *Synechocystis* sp. strain PCC 6803: identification of plasma membrane
761 proteins. Mol. Cell Proteomics 1:956–966
- 762 Kalscheuer, R., Stöveken, T., Malkus, U., Reichelt, R., Golyshin, P. N., Sabirova, J. S., Ferrer, M.,
763 Timmis, K. N., Steinbüchel, A (2007) Analysis of storage lipid accumulation in
764 *Alcanivorax borkumensis*: evidence for alternative triacylglycerol biosynthesis routes in
765 bacteria. J. Bacteriol. 189: 918–928.

- 766 Kornfeld, S., and Mellman, I (1989) The biogenesis of lysosomes. *Annu. Rev. Cell Biol.* 5,
767 483-525.
- 768 Keren, N., Liberton, M., and Pakrasi, H. B (2005) Photochemical competence of assembled
769 photosystem II core complex in cyanobacterial plasma membrane. *J. Biol. Chem.* 280:
770 6548–6553
- 771 Kim, P. K., Mullen, R. T., Schumann, U., and Lippincott-Schwartz, J (2006) The origin and
772 maintenance of mammalian peroxisomes involves a de novo PEX16-dependent pathway
773 from the ER. *J. Cell Biol.* 173: 521–532
- 774 Jian, Q. U., Zhang, C. M., and Zhai, Z. H (1994) Observation of nuclei reassembled from
775 demembranated *Xenopus* sperm nuclei and analysis of their lamina components. *Cell Res.*
776 4: 163–172
- 777 Johnstone, R. M., Adam, M., Hammond, J. R., Orr, L., and Turbide, C (1987) Vesicle formation
778 during reticulocyte maturation. Association of plasma-membrane activities with released
779 vesicles (exosomes). *J. Biol. Chem.* 262: 9412–9420
- 780 Jürgens, U. J., and Weckesser, J (1985) Carotenoid-containing outer membrane of *Synechocystis*
781 sp. strain PCC 6714. *J. Bacteriol.* 164:384–389.
- 782 Lang, N. J (1968) The fine structure of blue-green algae. *Ann. Rev. Microbiol.* 22: 15-46.
- 783 Lang, N. J., and Fisher, K. A (1969) Variation in the fixation image of "structural granules" in
784 *Anabaena*. *Arch. Mikrobiol.* 67: 173—181
- 785 Lea-Smith, D. L., Ross, N., Zori, M., Bendall, D. S., Dennis, J. S., Scott, S. A., Smith, A. G., Howe,
786 C. G (2013) Thylakoid terminal oxidases are essential for the cyanobacterium
787 *Synechocystis* sp. PCC6803 to survive rapidly changing light intensities. *Plant Physiol.*
788 162:484–495.
- 789 Lemasson, C., Marsac, N. T., and Cohen-Bazire, G (1973) Role of allophycocyanin as a
790 light-harvesting pigment in cyanobacteria. *Proc. Nat. Acad. Sci. USA* 70: 3130-3133.
- 791 Li, H. M., Kaneko, Y., and Keegstra, K (1994) Molecular cloning of a chloroplastic protein
792 associated with both the envelope and thylakoid membranes. *Plant Mol. Biol.* 25: 619–632.
- 793 Li, Y., Xu, M., Ding, X., Yan, C., Song, Z., Chen, L., Huang, X., Wang, X., Jian, Y., Tang, G., Tang,
794 C., Di, Y., Mu, S., Liu, X., Liu, K., Li, T., Wang, Y., Miao, L., Guo, W., Hao, X., Yang, C
795 (2016) Protein kinase C controls lysosome biogenesis independently of mTORC1. *Nat Cell*
796 *Biol.* 18:1065–1077.
- 797 Liberton, M., Berg, R. H., Heuser, J., Roth, R., and Pakrasi, H. B (2006) Ultrastructure of the
798 membrane systems in the unicellular cyanobacterium *Synechocystis* sp strain PCC 6803.
799 *Protoplasma* 227: 129–138

- 800 Lichtenthaler, H. K (1987) Chlorophylls and carotenoids: pigments of photosynthetic
801 biomembranes. *Methods Enzymol.* 148, 350–382.
- 802 Lichtenthaler, H. K (2013) Plastoglobuli, thylakoids, chloroplast structure and development of
803 plastids. In: Biswal B, Krupinska K, Biswal UC (eds) *Plastid development in leaves during*
804 *growth and senescence advances in photosynthesis and respiration.* Springer, Berlin, pp
805 337–361.
- 806 Liu, D. F., Xu, L., Yang, F., Li, D.D., Gong, F.L. and Xu, T (2005) Rapid biogenesis and
807 sensitization of secretory lysosomes in NK cells mediated by target-cell recognition. *Proc.*
808 *Natl. Acad. Sci. USA.* 102:123–127.
- 809 Lokha, M. J., and Masui, Y (1983) Formation in vitro of sperm pronuclei and mitotic
810 chromosomes induced by amphibian ooplasmic components. *Science* 220:719-21.
- 811 Lowe, M and Barr, F. A (2007) Inheritance and biogenesis of organelles in the secretory pathway.
812 *Nat. Rev. Mol. Cell. Biol.* 8:429–439.
- 813 Luzio, J. P, Hackmann, Y., Dieckmann, N. M., Griffiths, G. M (2014) The biogenesis of lysosomes
814 and lysosome-related organelles. *Cold Spring Harb. Perspect. Biol.* 6(9):a016840
- 815 Marty, F (1978) Cytochemical studies on GERL, provacuoles, and vacuoles in root meristematic
816 cells of *Euphorbia*. *Proc. Natl. Acad. Sci. USA* 75: 852–856.
- 817 Marty, F (1999) Plant vacuoles. *Plant Cell* 11:587-600
- 818 Mayor, S., and Pagano, R. E (2007) Pathways of clathrin-independent endocytosis. *Nat. Rev. Mol.*
819 *Cell Biol.* 8: 603–612
- 820 McMahon, H. T., and Boucrot, E (2011) Molecular mechanism and physiological functions of
821 clathrin-mediated endocytosis. *Nat. Rev. Mol. Cell Biol.* 12: 517–533
- 822 Meindl, U., Lancelle, S., and Hepler, P. K (1992) Vesicle production and fusion during lobe
823 formation in *Micrasterias* visualized by high-pressure freeze fixation. *Protoplasma*
824 170:104--114
- 825 Moore, L. R., Roca, G., and Chisholm, S. W (1998). Physiology and molecular phylogeny of
826 coexisting *Prochlorococcus* ecotypes. *Nature* 393: 464–467.
- 827 Motley, A. M., and Hettema, E. H (2007) Yeast peroxisomes multiply by growth and division. *J.*
828 *Cell Biol.* 178: 399–410
- 829 Mullineaux, C. W (2014) Co-existence of photosynthetic and respiratory activities in
830 cyanobacterial thylakoid membranes. *Biochim. Biophys. Acta* 1837: 503–511
- 831 Newport, J (1987) Nuclear reconstitution in vitro: Stages of assembly around protein-free DNA.
832 *Cell* 48:205-217
- 833 Nickel, W., and Rabouille, C (2009) Mechanisms of regulated unconventional protein secretion.

- 834 Nat. Rev. Mol. Cell Biol. 10:234-255
- 835 Olbrich, A., Hillmer, S., Hinz, G., Oliviusson, P., Robinson, D. G (2007) Newly formed vacuoles
836 in root meristems of barley and pea seedlings have characteristics of both protein storage
837 and lytic vacuoles. *Plant Physiol.* 145:1383-1394.
- 838 Opaliński, Ł., Bartoszevska, M., Fekken, S., Liu, H., de Boer, R., et al. (2012) De novo
839 peroxisome biogenesis in *Penicillium chrysogenum* is not dependent on the Pex11 family
840 members or Pex16. *PLoS ONE* 7: e35490. doi:10.1371/journal.pone.0035490
- 841 Osborn, M. J., Gander, J. E., Parisi, E., and Carson, J (1972) Mechanism of assembly of outer
842 membrane of *Salmonella typhimurium*: Isolation and characterization of cytoplasmic and
843 outer membrane. *J. Biol. Chem.* 247:3962-3972.
- 844 Packter, N. M., and Olukoshi, E. R (1995) Ultrastructural studies of neutral lipid localisation in
845 *Streptomyces*. *Arch. Microbiol.* 164:420-427
- 846 Pan, B.T., Teng, K., Wu, C., Adam, M., and Johnstone, R.M (1985) Electron microscopic evidence
847 for externalization of the transferrin receptor in vesicular form in sheep reticulocytes. *J.*
848 *Cell Biol.* 101:942-948
- 849 Paquet, V.E., Lessire, R., Domergue, F., Fouillen, L., Filion, G., Sedighi, A., Charette, S.J (2013)
850 Lipid composition of multilamellar bodies secreted by *Dictyostelium discoideum* reveals
851 their Amoebal origin. *Eukaryotic Cell* 12: 1326-1334.
- 852 Peltier, G., and Cournac, L (2002) Chlororespiration. *Annu. Rev. Plant Biol.* 53: 523-550.
- 853 Peramuna, A., and Summers, M. L (2014) Composition and occurrence of lipid droplets in the
854 cyanobacterium *Nostoc punctiforme*. *Arch. Microbiol.* 196: 881-890
- 855 Perera, R. M., and Zoncu, R (2016) The lysosome as a regulatory hub. *Annu. Rev. Cell Dev. Biol.*
856 32: 223-253
- 857 Peschek, G.A., Hinterstoisser, B., Wastyn, M., Kuntner, O., Plneau, E., Missblchler, A., and Lang,
858 J (1989) Chlorophyll precursors in the plasma membrane of a cyanobacterium *Anacystis*
859 *nidulans*. *J. Biol. Chem.* 264: 11827-11832.
- 860 Rabouille, C (2017) Pathways of unconventional protein secretion. *Trends Cell Biol.* 27:230-240
- 861 Ren, L., Mellander, L., Keighron, J., Cans, A. S., Kurczy, M., Svir, I., Oleinick, A., Amatore, C.,
862 Ewing, A. G (2016) The evidence for open and closed exocytosis as the primary release
863 mechanism. *Q. Rev. Biophys.* 49, e12.
- 864 Robinson, D.G, Ding, Y., and Jiang L. W (2016) Unconventional protein secretion in plants: a
865 critical assessment. *Protoplasma* 253: 31-43
- 866 Resch, C. M., and J. Gibson (1983) Isolation of the carotenoid-containing cell wall of three
867 unicellular cyanobacteria. *J. Bacteriol.* 155:345-350.

- 868 Rexroth, S., Mullineaux, C. W., Ellinger, D., Sendtko, E., Rögner, M., and Koenig, F (2011) The
869 plasma membrane of the cyanobacterium *Gloeobacter violaceus* contains segregated
870 bioenergetic domains. *Plant Cell* 23: 2379–2390.
- 871 Rippka, R., Waterbury, J., and Cohen-Bazire, G (1974) A cyanobacterium which lacks thylakoids.
872 *Arch. Microbiol.* 100: 419–436.
- 873 Robinow, C., and Kellenberger, E (1994) The bacterial nucleoid revisited. *Microbiol. Rev.*
874 58:211–232.
- 875 Rothman, J. E., and Wieland, F. T (1996) Protein sorting by transport vesicles. *Science* 272:
876 227–234.
- 877 Rossanese, O. W., Soderholm, J., Bevis, B. J., Sears, I. B., O'Connor, J., Williamson, E. K., and
878 Glick, B. S (1999) Golgi structure correlates with transitional endoplasmic reticulum
879 organization in *Pichia pastoris* and *Saccharomyces cerevisiae*. *J. Cell Biol.* 145:69–81
- 880 Rucktaschel, R., Halbach, A., Girzalsky, W., Rottensteiner, H., and Erdmann, R (2010) De novo
881 synthesis of peroxisomes upon mitochondrial targeting of Pex3p. *Eur. J. Cell Biol.* 89,
882 947–954
- 883 Saftig P., and Klumperman, J (2009) Lysosome biogenesis and lysosomal membrane proteins:
884 trafficking meets function. *Nat. Rev. Mol. Cell Biol.* 10: 623–635
- 885 Samuels, A. L., Giddings, T. H., and Staehelin, L. A (1995) Cytokinesis in tobacco BY-2 and root
886 tip cells: a new model of cell plate formation in higher plants. *J. Cell Biol.* 130: 1345–1357
- 887 Schatz, G., and Dobberstein, B (1996) Common principles of protein translocation across
888 membranes. *Science* 271:1519–1526.
- 889 Schekman, R., and Orci, L (1996) Coat proteins and vesicle budding. *Science* 271: 1526–1533.
- 890 Shively, J. M., Ball, F., Brown, D. H., and Saunders, R. E (1973) Functional organelles in
891 prokaryotes: polyhedral inclusions (carboxysomes) of *Thiobacillus neapolitanus*. *Science*
892 182: 584–586
- 893 Simon, R. D (1971) Cyanophycin granules form the blue-green alga *Anabaena cylindrica*: a
894 reserve material consisting of copolymers of aspartic acid and arginine. *Proc. Natl. Acad.*
895 *Sci. USA* 68:265–267.
- 896 Smith, D., and Howe, C. J (1993) The distribution of Photosystem I and Photosystem II
897 polypeptides between the cytoplasmic and thylakoid membranes of cyanobacteria. *FEMS*
898 *Microbiol. Lett.* 110: 341-348
- 899 Smith, M. D., Licatalosi, D. D., and Thompson, J. E (2000) Co-association of cytochrome f
900 catabolites and plastid-lipid-associated protein with chloroplast lipid particles. *Plant*
901 *Physiol.* 124: 211–222

- 902 South, S. T., and Gould, S. J (1999) Peroxisome Synthesis in the Absence of Preexisting
903 Peroxisomes. *J. Cell Biol.* 144: 255–266
- 904 Srivastava, R., Battchikova, N., Norling, B., and Aro, E.M (2006) Plasma membrane of
905 *Synechocystis* PCC 6803: A heterogeneous distribution of membrane proteins. *Arch.*
906 *Microbiol.* 185: 238–243.
- 907 Stanier, R. Y., Kunisawa, R., Mandel, M., and Cohen-Bazire, G. (1971). Purification and properties
908 of unicellular blue-green algae (Order Chroococcales). *Bacteriol. Rev.* 35: 171–205.
- 909 Sugiura, A., Mattie, S., Prudent, J., and McBride, H. M (2017) Newly born peroxisomes are a
910 hybrid of mitochondrial and ER-derived pre-peroxisomes. *Nature* 542: 251–254
- 911 T ängemo, C., Ronchi, P., Colombelli, J., Haselmann, U., Simpson, J.C., Antony, C., Stelzer,
912 E.H.K., Pepperkok, R., and Reynaud, E.G (2010) A novel laser nanosurgery approach
913 supports de novo Golgi biogenesis in mammalian cells. *J. Cell Sci.* 124: 978–987
- 914 Th éry, C., Zitvogel, L., and Amigorena, S (2002) Exosomes: composition, biogenesis and function.
915 *Nat. Rev. Immunol.* 2: 569–579
- 916 Thorne, S.W., Newcomb, E.H., and Osmond, C.B (1977) Identification of chlorophyll b in extracts
917 of prokaryotic algae by fluorescence spectroscopy. *Proc. Natl. Acad. Sci. USA* 74:
918 575–578.
- 919 van der Zand, A., Gent, J., Braakman, I., and Tabak, H. F (2012) Biochemically distinct vesicles
920 from the endoplasmic reticulum fuse to form peroxisomes. *Cell* 149: 397–409.
- 921 van de Meene, A. M., Hohmann-Marriott, M. F., Vermaas, W. F., Roberson, R. W (2006) The
922 three-dimensional structure of the cyanobacterium *Synechocystis* sp. PCC 6803. *Arch.*
923 *Microbiol.* 184: 259–270
- 924 van Doorn, W. G., Kirasak, K., and Ketsa, S (2015) Macroautophagy and microautophagy in
925 relation to vacuole formation in mesophyll cells of *Dendrobium tepals*. *J. Plant Physiol.*
926 177: 67–73
- 927 van Doorn, W. G., and Papini, A (2013) Ultrastructure of autophagy in plant cells. *Autophagy*
928 9:1922–1936
- 929 Vidi, P., Kanwischer, M., Baginsky, S., Austin, J. R., Csucs, G., D örmann, P., Kessler, F., and
930 Br ř ě ě in, C (2006) Tocopherol cyclase (VTE1) localization and vitamin E accumulation in
931 chloroplast plastoglobule lipoprotein particles. *J. Biol. Chem.* 281: 11225–11234
- 932 Vigers, G. P., and Lohka, M. J (1991) A distinct vesicle population targets membranes and pore
933 complexes to the nuclear envelope in *Xenopus* eggs. *J. Cell Biol.* 112, 545–556.
- 934 Viotti, C., et al. (2013) The endoplasmic reticulum is the main membrane source for biogenesis of
935 the lytic vacuole in *Arabidopsis*. *Plant Cell* 25:3434–3449.

- 936 Waterbury, J. B., and Stanier, R. Y (1978) Patterns of growth and development in Pleurocapsalean
937 cyanobacteria. *Microbiol. Rev.* 42: 2-44
- 938 Westphal, S., Heins, L., Soll, J., and Vothknecht, U. C (2001) Vipp1 deletion mutant of
939 *Synechocystis*: a connection between bacterial phage shock and thylakoid biogenesis? *Proc.*
940 *Natl. Acad. Sci. USA* 98: 4243–4248.
- 941 Yeates, T. O., Kerfeld, C. A., Heinhorst, S., Cannon, G. C., and Shively, J. M (2008) Protein-based
942 organelles in bacteria: carboxysomes and related microcompartments. *Nat. Rev. Microbiol.*
943 6: 681–691
- 944 Ytterberg, A. J., Peltier, J., and van Wijk, K. J (2006) Protein profiling of plastoglobules in
945 chloroplasts and chromoplasts. A surprising site for differential accumulation of metabolic
946 enzymes. *Plant Physiol.* 140: 984–997
- 947 Zak, E., Norling, B., Maitra, R., Huang, F., Andersson, B., and Pakrasi, H. B (2001) The initial
948 steps of biogenesis of cyanobacterial photosystems occur in plasma membranes. *Proc. Natl.*
949 *Acad. Sci. USA* 98:13443–13448
- 950 Zhang, M., and Schekman, R (2013) Cell biology. Unconventional secretion, unconventional
951 solutions. *Science* 340:559-561.
- 952 Zhang, S., Shen, S., Li, Z., Golbeck, J. H., and Bryant, D.A (2014) Vipp1 is essential for
953 biogenesis of Photosystem I but not thylakoid membranes in *Synechococcus* sp. PCC7002.
954 *J. Biol. Chem.* 289: 15904–15914.

955 **Acknowledgements**

956 This work was supported by the Natural Science Foundation of Hebei Province (B2008000029).

957 **Author contributions**

958 Q.L.D and X.Y.X. performed the experiment and wrote the manuscript with the participation of
959 Y.H in partial electron microscopic observation and 16S rRNA sequencing, X.L.W and S. Z in
960 pigment analyses.

961

962

963

964

965

966

967

968 **List of abbreviations**

AUG	Autosporangium	EW	Eukaryotic cell wall
C	Chloroplast	FM	Fibrillary materials
CD	Chloroplast debris	GA	Golgi apparatus
CE	Cytoplasmic envelope	GP	Globular particles
CF	Chromatin fibers	HGB	Heterogenous globular bodies
CG	Cyanophycin granules	IB	Intranuclear body
CHE	Chloroplast envelope	ICE	Intracytoplasmic envelope
CLM	Cloudlike materials	ICP	Inner cytoplasm
CM	Cytoplasmic membrane	IES	Inter envelope space
CPV	Compound vesicles	IIM	Inner intracytoplasmic membrane
CR	Cristae	IIS	Inner intracytoplasmic space
CV	Combined vesicles	INS	Interspace
CW	Cell wall	IS	Intracytoplasmic space
CX	Carboxysomes	ITB	Internal body
DF	DNA Fibers	IV	Internal vesicle
DGV	Dense-margined vesicles	IVS	Invaginated space
DLF	DNA-like fibrils	LD	Lipid droplet
DMF	Double-layered membrane fragment	LDB	Less electron-dense bodies
DMS	Double-layered membrane segment	LDM	Less electron-dense materials
DMV	Double-membraned vesicles	LM	Limiting membrane
DRV	Dilated ring-shaped vesicles	M	Mitochondrion
DSV	Dense vesicle	ME	Mitochondrial envelope
DT	DNA threads	MF	Membrane fragments
DV	Dotted vesicles	ML	Microfibrils
ED	Electron-dense debris	MLB	Multilamellar body
EDV	Electron-dense vesicles	MR	Margin residues
EF	Electron-dense fibrils	MS	Membrane segments
EG	Electron-dense granules	MT	Membranous elements
EIS	Empty Inner space	MV	Microvesicles
EL	Electron-dense layer	N	Nucleus
ELM	Electron-translucent materials	NE	Nuclear envelope
ELV	Electron-translucent vesicles	NIC	New inner cytoplasm
EM	Eukaryotic cytoplasm	NIS	New inner intracytoplasmic space
EOB	Electron-opaque bodies	NS	New intracytoplasmic space
EOP	Electron-opaque particles	NT	Nucleoid-like structure
EOM	Electron-opaque materials	NU	Nucleoid
EOV	Electron-opaque vesicles	NX	New intracytoplasmic matrix
EP	Electron-dense particles	OCP	Outer cytoplasm
EPM	Electron-transparent materials	OE	Outer nuclear envelope
ER	Endoplasmic reticulum	OG	Osmiophilic granules
ES	Extracytoplasmic space	OIM	Outer intracytoplasmic membrane
EV	Electron-transparent vesicle	OIS	Outer intracytoplasmic space

OPV	Opaque-periphery vesicle	SA	Sporangium
OM	Outer membrane	SG	Starch granules
OV	Oblong vesicles	SH	Sheath
P	Peptidoglycan layer	SMV	Smaller vesicles
PB	Polyphosphate bodies	SM	Stroma
PC	Primitive chloroplast	SOV	Small opaque vesicle
PCB	Phycobilisomes	SP	Starch plate
PD	Pyrenoids	ST	Secondary thylakoids
PG	Plastoglobuli	SV	Small vesicles
PL	Peptidoglycan-like layer	T	Thylakoids
PMT	Primitive thylakoids	TE	Tubules
PN	Primitive nucleus	TL	Thylakoid-like structure
PNE	Primitive nuclear envelope	TMF	Two-layered membrane fragment
PO	Pores	TMV	Thick margin vesicle
PT	Primary thylakoids	TV	Tiny vesicles
RB	Ribosomes	V	Vacuole
RM	Residual membranes	VB	Vesicle-containing body
RV	Ring-shaped vesicles		

Figures

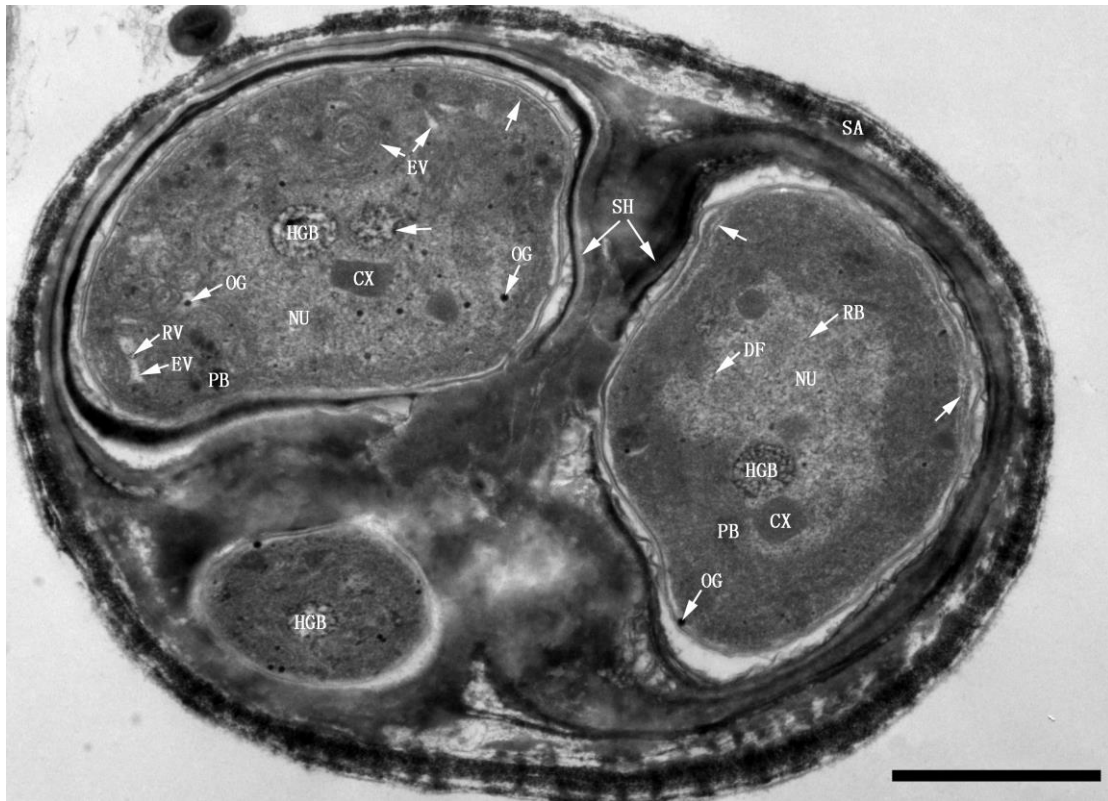


Figure1. Three TDX16 cells within a sporangium (SA). TDX16 cells were enclosed by thick sheaths (SH), containing no organelle and thylakoid, but unique heterogenous globular bodies (HGB), carboxysomes (CX), ribosomes (RB), DNA fibers (DF) and osmiophilic granules (OG) in the nucleoids (NU) as well as polyphosphate bodies (PB) in the cytoplasm. OG also presented in cytoplasm and some small electron-transparent vesicles (EV) with internal ring-shaped vesicles (RV) or OG were being formed in the upper left cell. Compartmentalization was just initiated in the two large cells (arrow). Scale bar, 1 μ m.

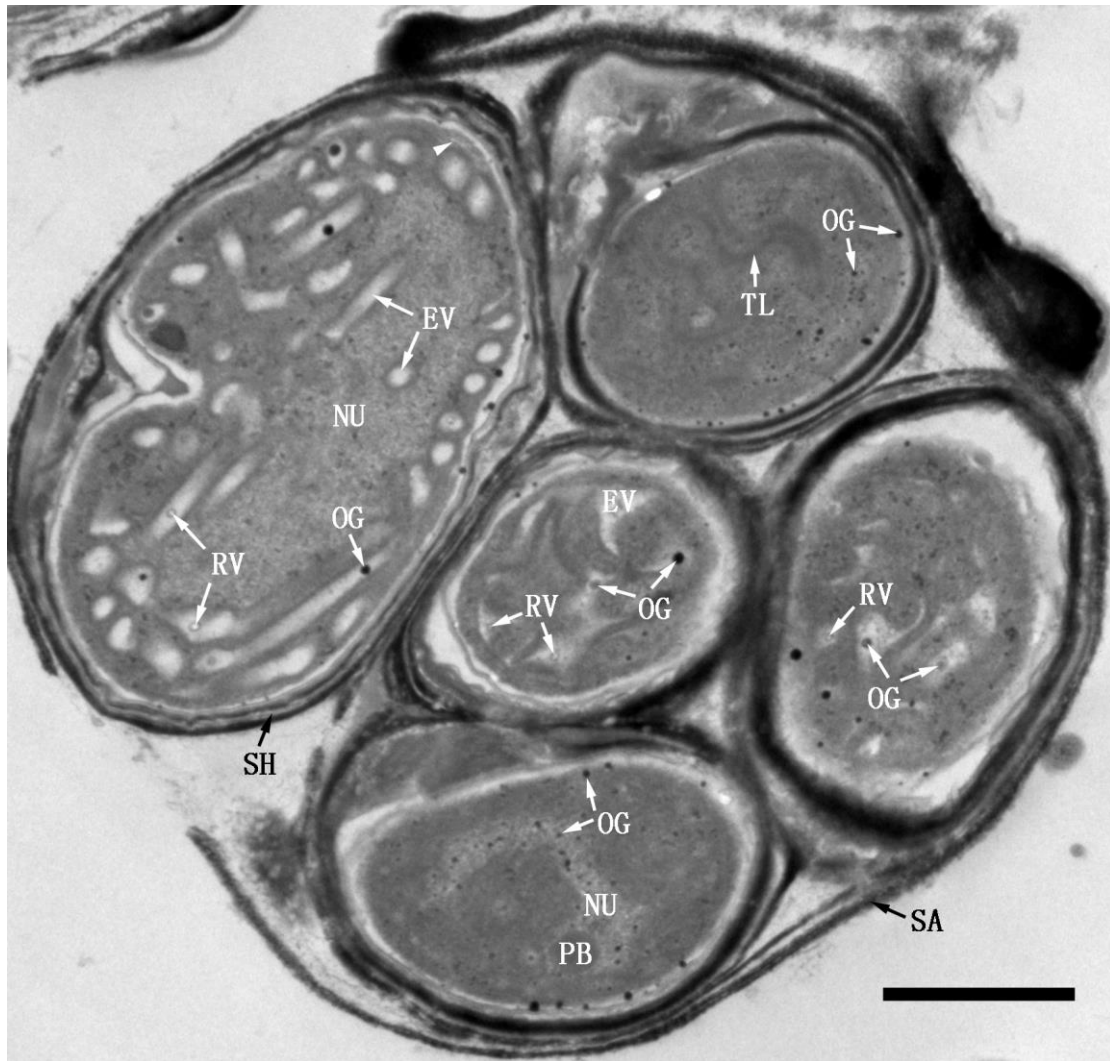


Figure 2. Five TDX16 cells within a SA. The bottom cell was devoid of EV, while a great number of EV were being developed in the three middle cells, and several thylakoid-like structures (TL) were built up in the upper cell. Compartmentalization commenced in the large cell (arrowhead). Scale bar, 1 μ m.

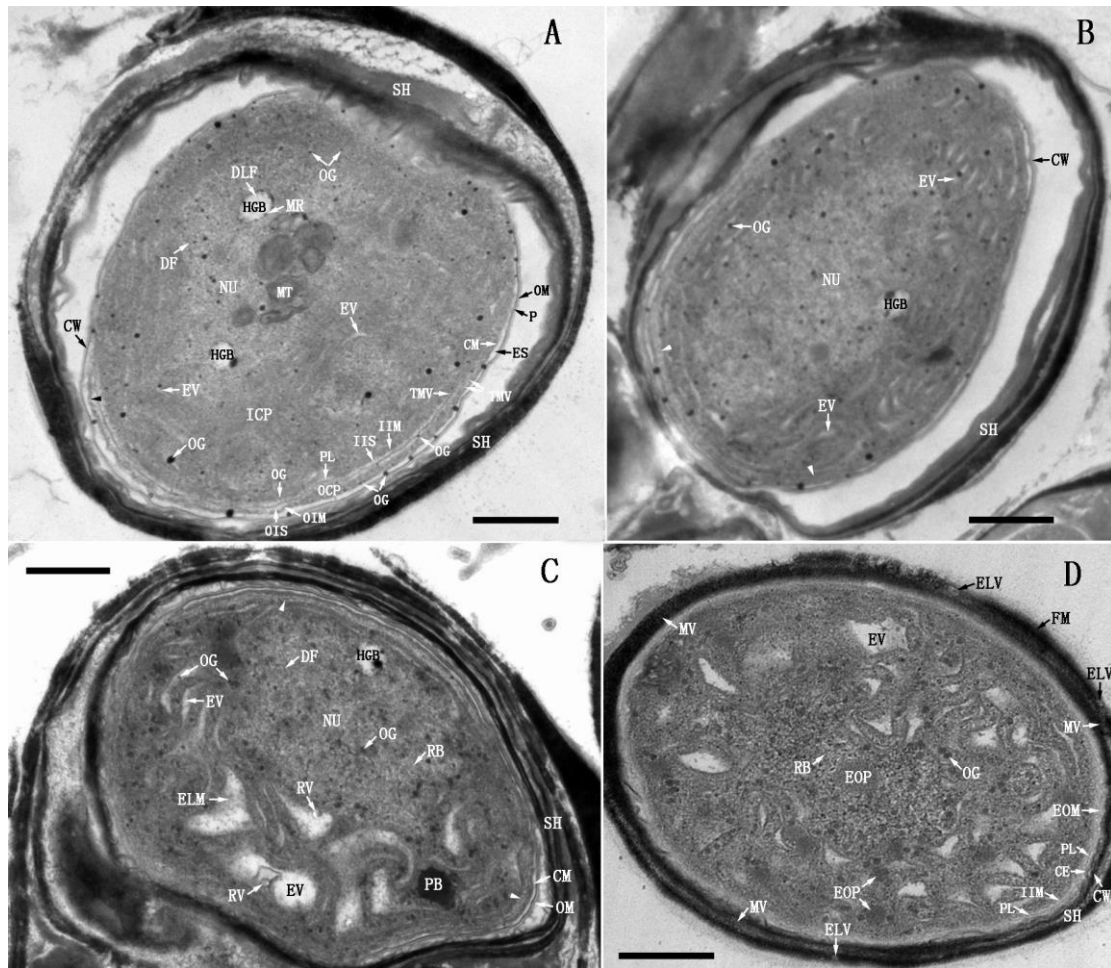


Figure 3. Compartmentalization, formation of EV and cytoplasmic envelope. (A) TDX16's cell wall (CW) comprised an outer membrane (OM) and a peptidoglycan layer (P), which was separated from the cytoplasmic membrane (CM) by an extracytoplasmic space (ES). Inside the cytoplasm, an inner intracytoplasmic membrane (IIM), an outer intracytoplasmic membrane (OIM) and an intervening peptidoglycan-like layer (PL) were being synthesized by fusion of the small thick margin vesicles (TMV) blistered form the inner leaflet of the cytoplasmic membrane. Whereby, the cytoplasm was partitioned into three compartments: the inner cytoplasm (ICP); the outer cytoplasm (OCP), and the sandwiched intracytoplasmic space (IS) that was further separated by PL into an outer intracytoplasmic space (OIS) and an inner intracytoplasmic space (IIS). OCP began to reduce in localized region near the start point (arrowhead), such that OIM moved to CM. OG budded from the inner leaflet of CM, IIM and OIM, and migrated into ICP, where many small EV were being formed and stacks of membranous elements (MT) emerged; while HGB became nearly empty leaving only DNA-like fibrils (DLF) and electron-dense margin residues (MR). Interestingly, OG shed from the outer leaflet of CM into ES, connecting CM and CW. (B) IS became narrow (arrow), while more and more small EV were being developed from OG. (C) EV dilated into swirling ones spiraling around NU, but IS still remained narrow. (D) When EV was formed in NU, several electron-opaque particles (EOP) emerged, while IS became widened filling with electron-opaque materials (EOM). Importantly, OCP disappeared such that OIM and CM were positioned together, and became a double-membraned cytoplasmic envelope (CE). Some electron-dense materials were synthesized on CE and transferred to CW for assembling SH, which was made up of flocculent fibrillary materials (FM), microvesicles (MV) and electron-translucent vesicles (ELV). Scale bar, 0.5 μ m.

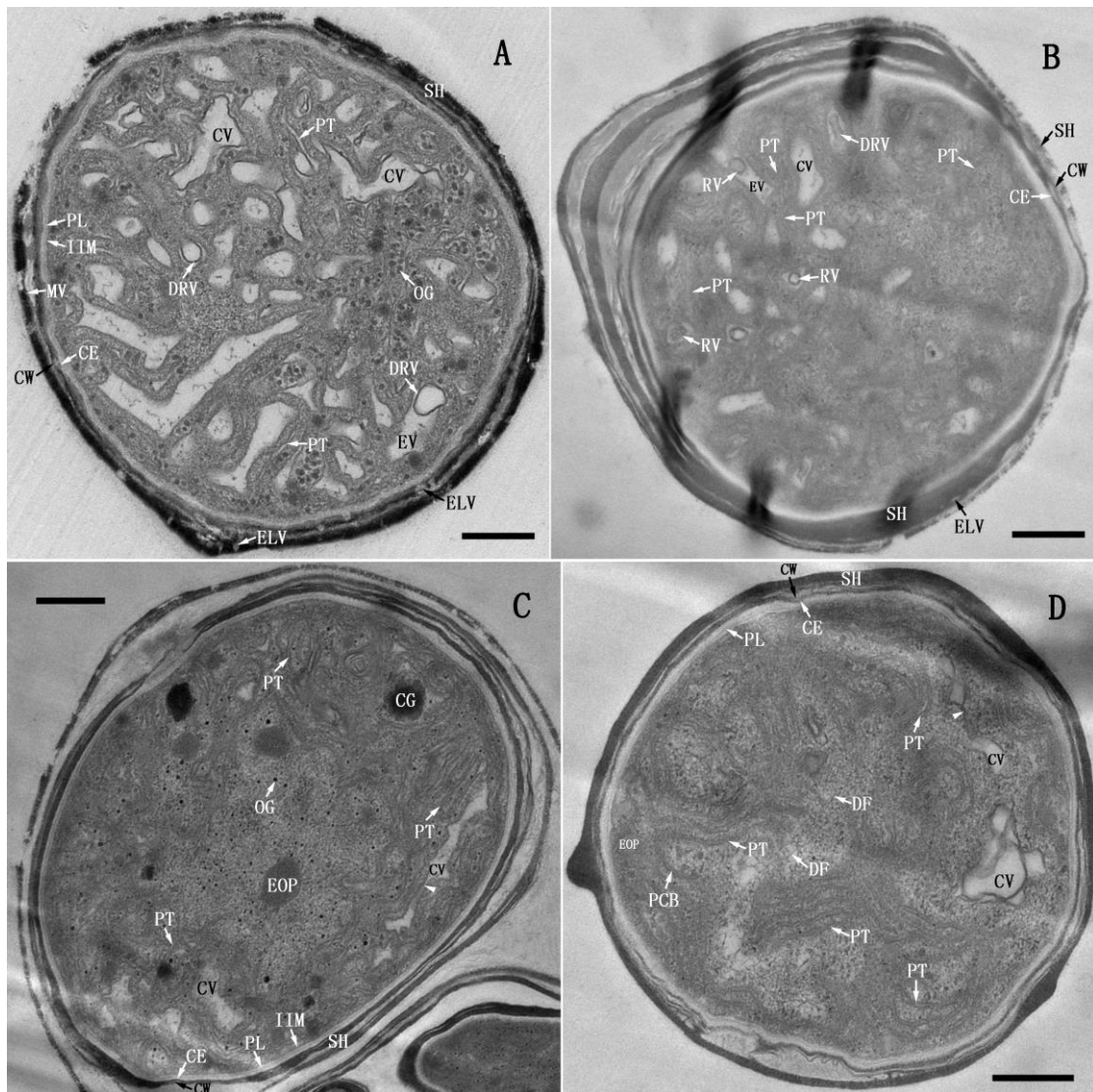


Figure 4. Development of EV into primary thylakoid. (A) RV swelled into dilated-ring-shaped vesicle (DRV), whose membrane met ultimately with EV membrane, and thus gave rise to a unit-membrane-bounded combined vesicle (CV). Subsequently, CV coalesced into longer ones or flattened out into slender short primary thylakoids (PT). (B) The newly formed short PT distributed randomly in ICP, whose matrix turned opaque. Occasionally a cluster of small RV presented in a EV. (C) The short PT extended or merged end-to-end into long PT; while the long coalesced CV flattened out into PT by localized-constriction (arrowhead). Meanwhile, several cyanophycin granules (CG) were formed. (D) PT became parallel-arranged with wide spacing, on which the extrinsic phycobilisomes (PCB) were assembled. Scale bar, 0.5 μm .

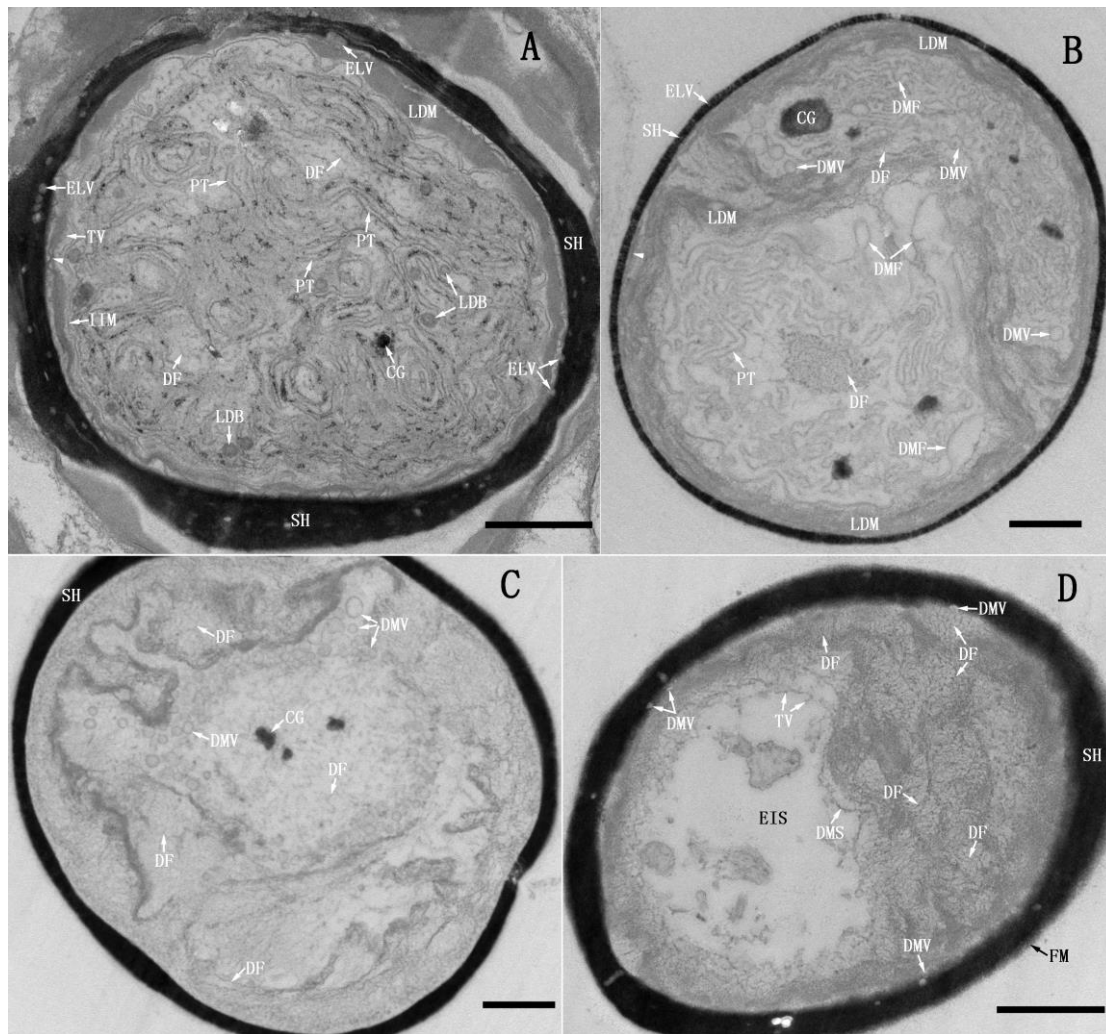


Figure 5. Decondensation of ICP, disassembly of IIM and PT, and translocation of DNA. (A) IIM broke down and rounded up into tiny vesicles (TV); PT matrix condensed and thus the membrane pair were in close apposition with concurrent disassembly of PCB; ICP decondensed and became translucent, in which short DF dispersed, and some less electron-dense materials (LDM) and less electron-dense bodies (LDB) were formed. LDM diffused outward and blurred the compacted PL, CE and CW (arrowhead). (B) PT broken up into double-layered membrane fragments (DMF), which began to merge laterally into double-membraned vesicles (DMV); while DF aggregated into a cluster. (C) All PT transformed into DMV, dispersing along with the aggregated DNA fibers in the decondensed ICP. (D) DMV moved outward quickly and attached to PL that was cover by electron-dense materials, while the intermingled DF scattered outward slowly resulting in an “empty” inner space (EIS), at the border of which the recruited TV began to fuse and elongate into double-layered membrane segments (DMS). Scale bar, 0.5 μ m.

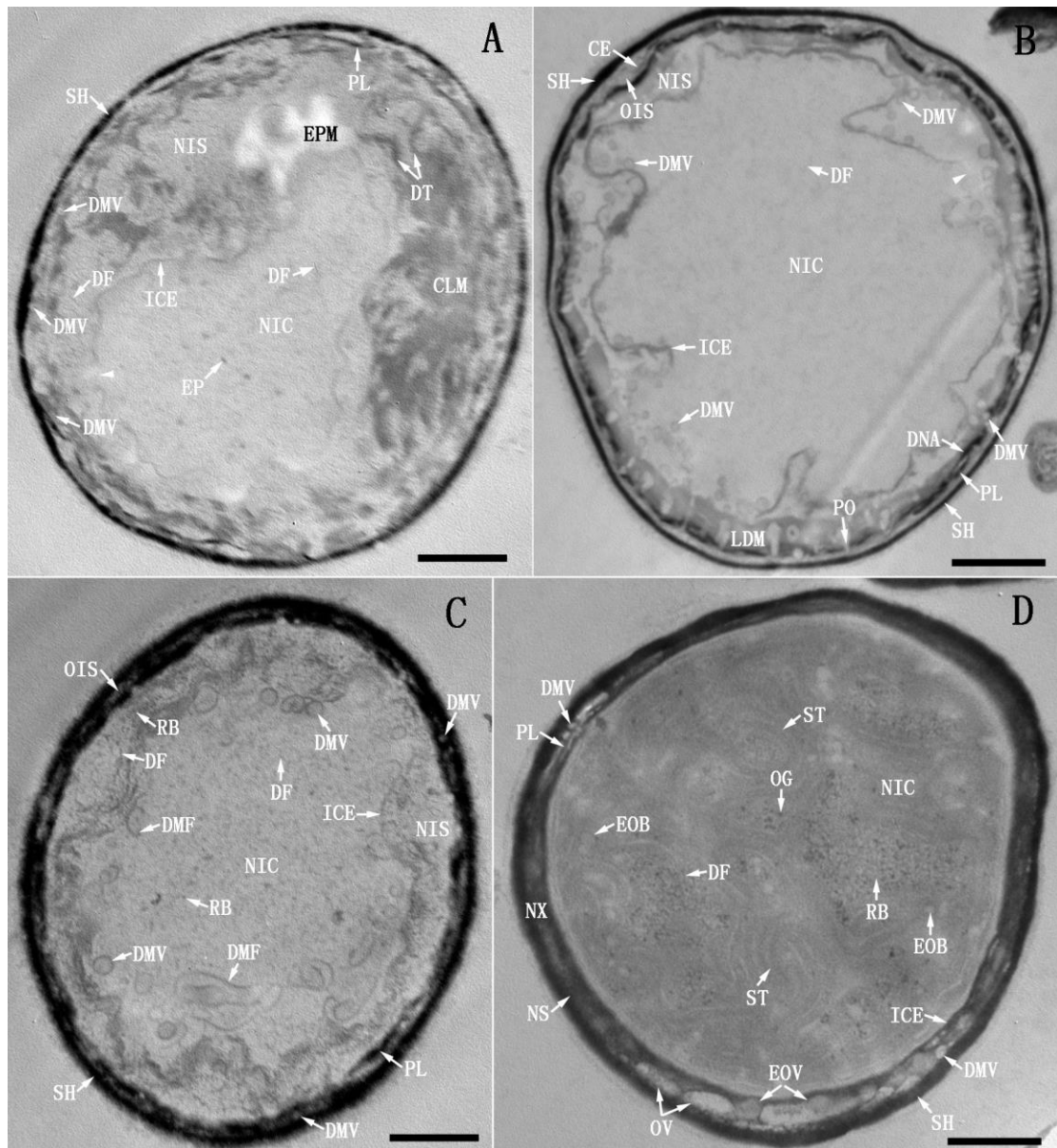


Figure 6. Re-compartmentalization, reallocation of DNA and formation of secondary thylakoids. (A) As DMS extended into a double-membraned intracytoplasmic envelope (ICE), a new inner cytoplasm (NIC) and a new inner intracytoplasmic space (NIS) were re-compartmentalized. Most of the DNA fibers were relocated in NIS, which decondensed into cloudlike materials (CLM) or aggregated into DNA threads (DT). By contrast only few DF and electron-dense particles (EP) were partitioned into NIC. ICE was not sealed, so substances could be exchanged through its opening (arrowhead). Interestingly, some electron-transparent materials (EPM) were synthesized on the outer leaflet of ICE. (B) Accompanying the expansion of ICE, DMV in NIS moved into NIC via ICE opening (arrowhead), or passed through PL pores (PO) into OIS. (C) After ICE sealed, DNA in NIS recondensed into a mass of DF with concomitant formation of countless RB. Meanwhile, an increased number of DF emerged and some RB were formed in NIC; DMV began to open up and re-transformed into DMF and elongated. (D) DMF in NIC extended into PCB-less secondary thylakoids (ST) with concomitant formation of OG and electron-opaque bodies (EOB) as well as enrichment of DF and RB. Outside of NIC, the major portion of PL was dismantled, such that NIS and OIS coalesced into a new intracytoplasmic space (NS), whose confluent content became the new intracytoplasmic matrix (NX). Aside from DMV, electron-translucent oblong vesicles (OV) and electron-opaque vesicles (EOV) emerged in NS. Scale bar, 0.5 μ m.

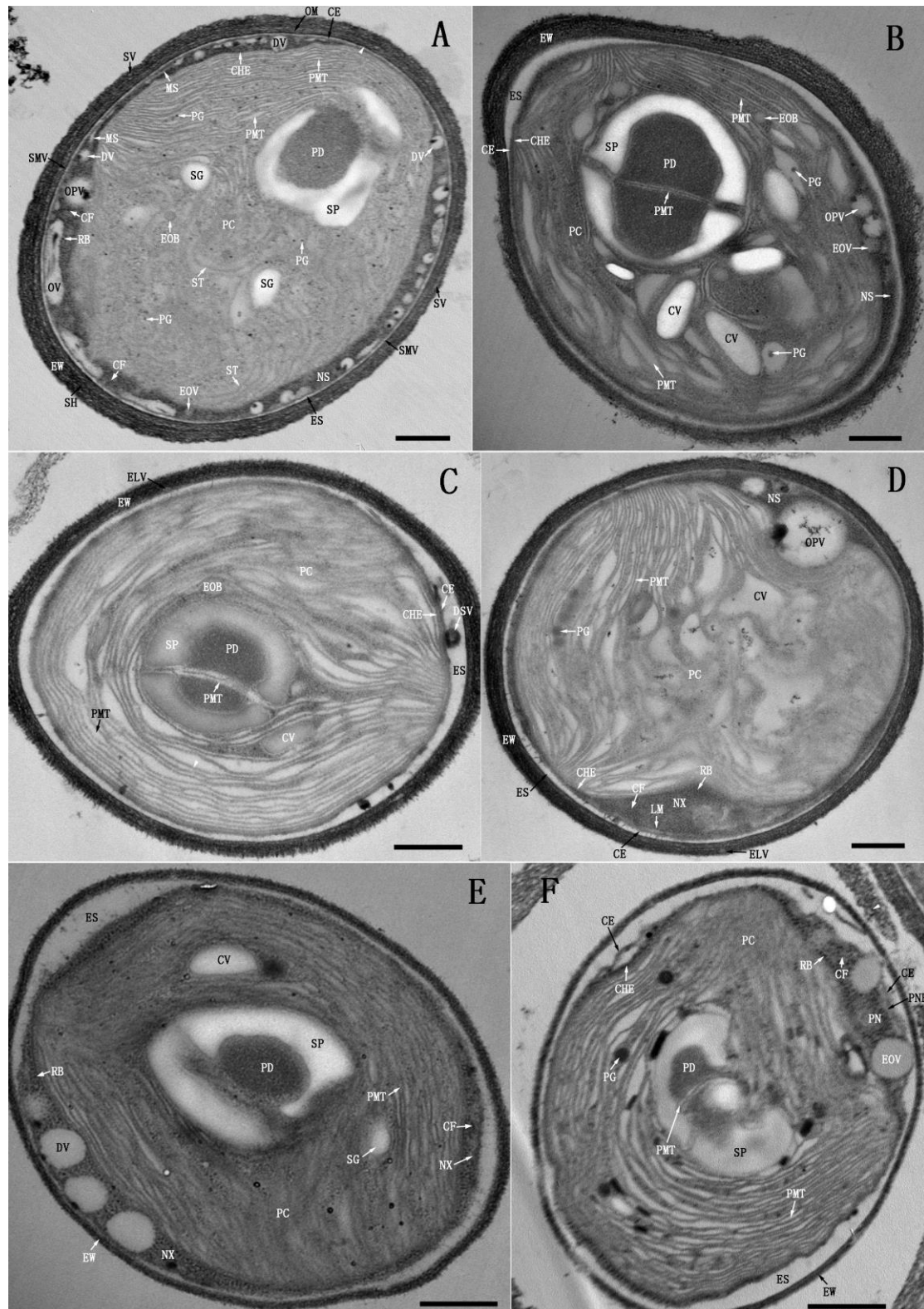


Figure 7. Biogenesis of primitive chloroplast, eukaryotic cell wall and primitive nucleus. (A) ST was disassembled leaving some remnants in the lower region of the polarized NIC, while parallel arrays of primitive eukaryotic thylakoids (PMT) were being developed from the plastoglobuli (PG) in upper region of NIC with concomitant formation of a nascent pyrenoid (PD) surrounding by an incomplete starch plate (SP), and two starch granules (SG). So, NIC developed into the primitive chloroplast (PC), and ICE became the chloroplast envelope

(CHE). Inside NS, thick chromatin fibers (CF) and large RB were formed; PL and DMV disappeared; while many small dotted vesicles (DV) and opaque-periphery vesicle (OPV) emerged. Some DV began to fuse and flattened into membrane segments (MS). Outside of NS, some smaller vesicles (SMV) shed from the outer leaflet of CE into ES; while the peptidoglycan layer (P) of CW turned into an electron-dense layer (EL) (arrowhead), and a stratified SH embedded with small vesicles (SV) was formed external to OM, hence the compacted CW and SH became the eukaryotic cell wall (EW). **(B)** PMT with wide luminal space were formed continuously by elongation of CV; PD got matured with a complete SP, bisecting by two pairs of PMT. The expanded PC occupied most of NS in longitudinally sectioned plane. **(C)** PC filling with PMT occupied whole NS, such that NS disappeared in longitudinally sectioned plane, CHE adhered to CE, from which a dense vesicle (DSV) shed off into the widened ES. **(D)** A vertical section of cell. The anterior PC portion occupied the surrounding NS, so EX was pushed to the shrinking NS around the posterior portion of PC, at the border of which MS fused into a limiting membrane (LM). **(E)** An oblique section through the posterior half of cell, in which most of the NX aggregated at one side of PC. **(F)** A tangential section through the posterior end of cell. All NX converged at one side of PC, which was encased by LM and thus turned into the primitive nucleus (PN) containing CF, RB and EOVS; while LM became the primitive nuclear envelope (PNE). NS vanished and in turn CE shrank and wrapped PC and PN. Scale bar, 0.5 μm .

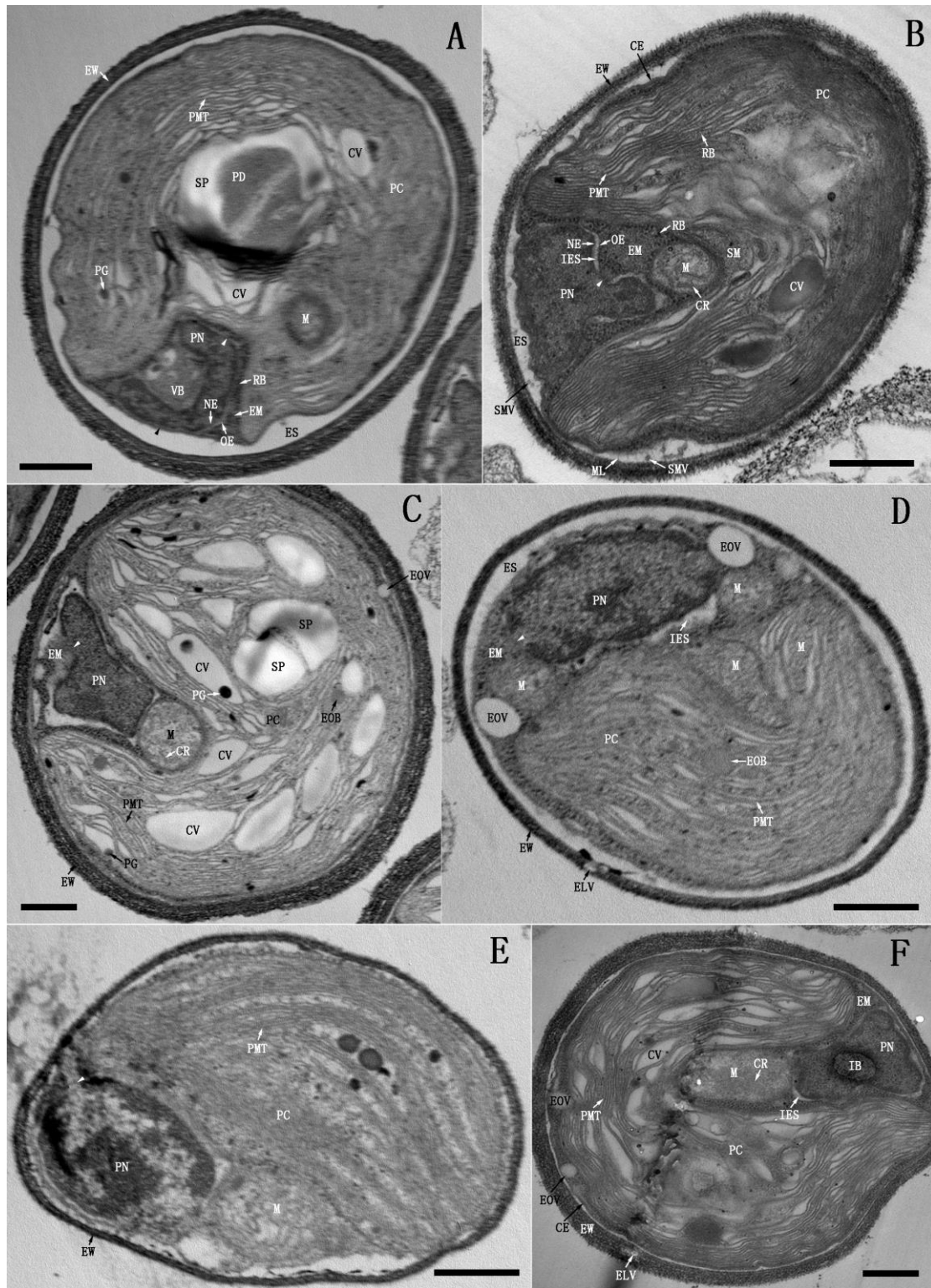


Figure 8. Concurrent formation of eukaryotic cytoplasm and biogenesis of mitochondria. (A) PN was engulfing a vesicle-containing body (VB) with concomitant extrusion of nuclear matrix, i.e. the eukaryotic cytoplasm (EM). PNE comprised a nuclear envelope (NE) and an outer nuclear envelope (OE), which was contiguous with CE at the outer side (black arrowhead), but separated in PC cavity. EM was extruded from PN at the site where NE and OE fused (white arrowhead), and concurrently a mitochondrion (M) was assembled in PC. (B) PC with enriched stroma (SM) further invaginated, in the apical dome of its cavity, a mitochondrion with

characteristic cristae (CR) emerged. OE and NE of the enlarged PN were separated by an inter envelope space (IES), but came into contact at one site and fused into a large opening (arrowhead), from which the nuclear matrix (i.e. EM) was expelled. In the meantime, a number of SMV and microfibrils (ML) budded and emanated from CE into ES. (C) PN expelled EM from the fused opening of NE and OE (arrowhead) in the presence of a newly formed spherical mitochondrion. (D) A large PN extruded EM (arrowhead) in the presence of two mitochondria, while two spindle-shaped mitochondria were being assembled within PC. (E) PN expelled EM (arrowhead) coincident with the appearance of a spindle-shaped mitochondrion. (F) A large PN contained a membrane-delimited intranuclear body (IB). Scale bar, 0.5 μm .

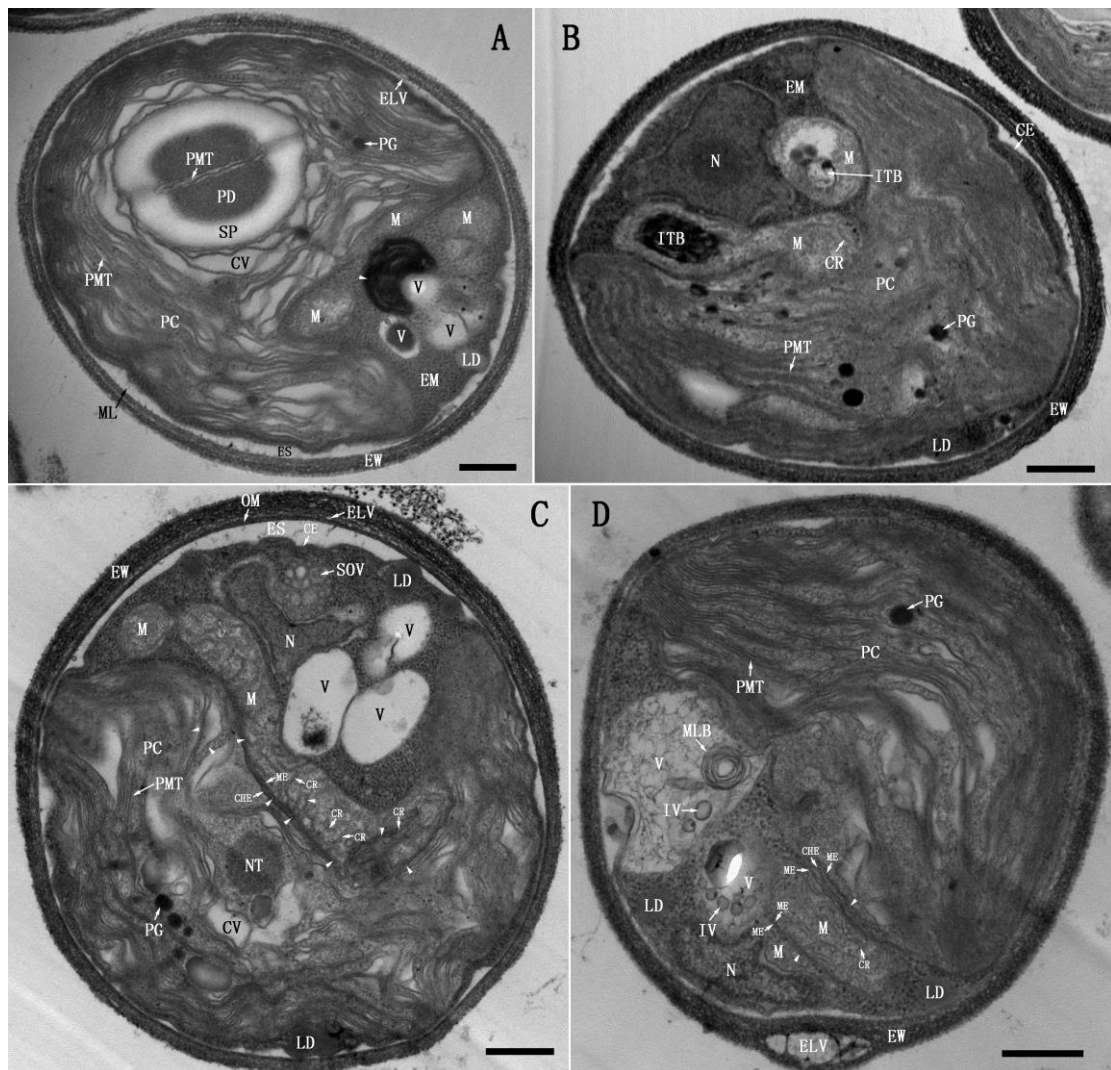


Figure 9. Biogenesis of mitochondria after building up EM. (A) After formation of EM, PN got matured into nucleus (N); while a small mitochondrion was being developed in PC in the presence of two mitochondria, three vacuoles (V), a lipid droplet (LD) and some electron-dense materials (arrowhead). (B) A twisting dumbbell-shaped mitochondrion was nearly finished, one of its bulbous-end containing an internal body (ITB) was segregated, but the other was contiguous with PC. Another mitochondrion within EM also sequestered an ITB. (C) A large ‘L-shaped’ mitochondrion was being assembled in the presence of three vacuoles and a cluster of small opaque vesicles (SOV), which was continuous with PC in the region around its corner point. The inner side mitochondrial envelope (ME) and the corresponding portion of CHE as well as CR were all synthesized by fusion of the dense-margined vesicles (DGV) (arrowhead) that were developed by segmentation of PMT. There was a large nucleoid-like structure (NT) in the venter side of PC. (D) After emergence of the large vacuoles with internal vesicle (IV) and multilamellar body (MLB), a bulky mitochondrion was being developed, which was connected with PC on the inner side but a small mitochondrion on the outer side. In the inner and outer interfaces, three and two pairs of contorted membranes were being synthesized respectively by merging DGV (arrowhead). In addition, several large ELV were embedded in EW. Scale bar, 0.5 μm .

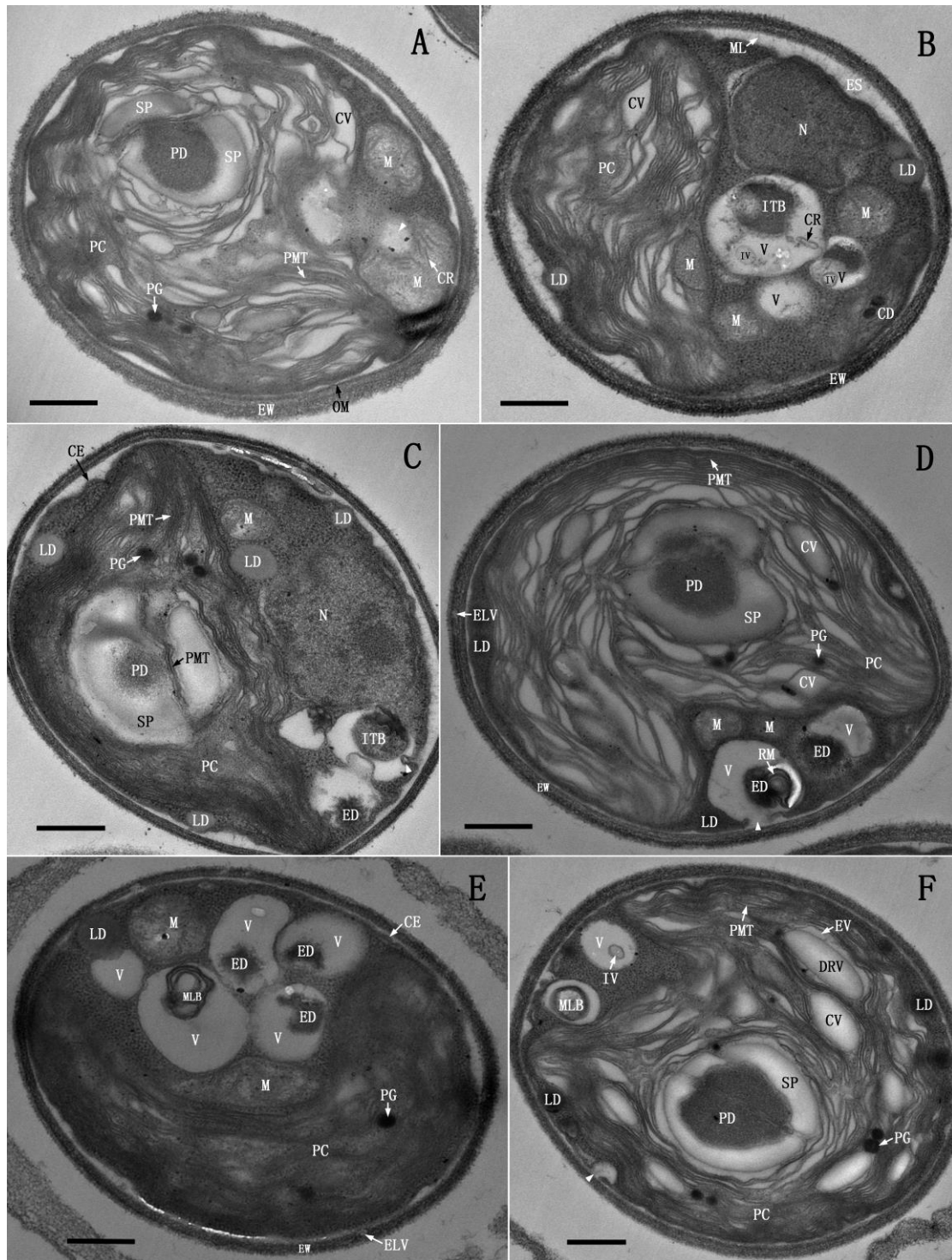


Figure 10. Biogenesis of vacuoles (A) The matrix of a mitochondrion was being degraded (arrowhead). (B) After matrix degradation, the mitochondrion turned into a vacuole containing ITB, IV and remnant CR or only electron-transparent matrix. Meanwhile, a new mitochondrion was being developed in PC, a LD was formed at CE and a piece of chloroplast debris (CD) emerged in EM. (C) ITB in two small mitochondria degraded into electron-dense debris (ED); while ITB in the large vacuole remained intact, the vacuolar membrane fused with CE and invaginated (arrowhead) (D) a small vacuole expelled ED into EM; while a large vacuole sequestered some residual membranes (RM), the membranes of which contacted and fused with CE, resulting in an opening

(arrowhead). (E) A large vacuole contained MLB, while a small vacuole extruded a LD into EM. (F) Two vacuoles contained MLB and IV respectively. A small vacuole fused with CE, giving rise to an opening (arrowhead); and several cobblestone-shaped DRV emerged in EV. Scale bar, 0.5 μm .

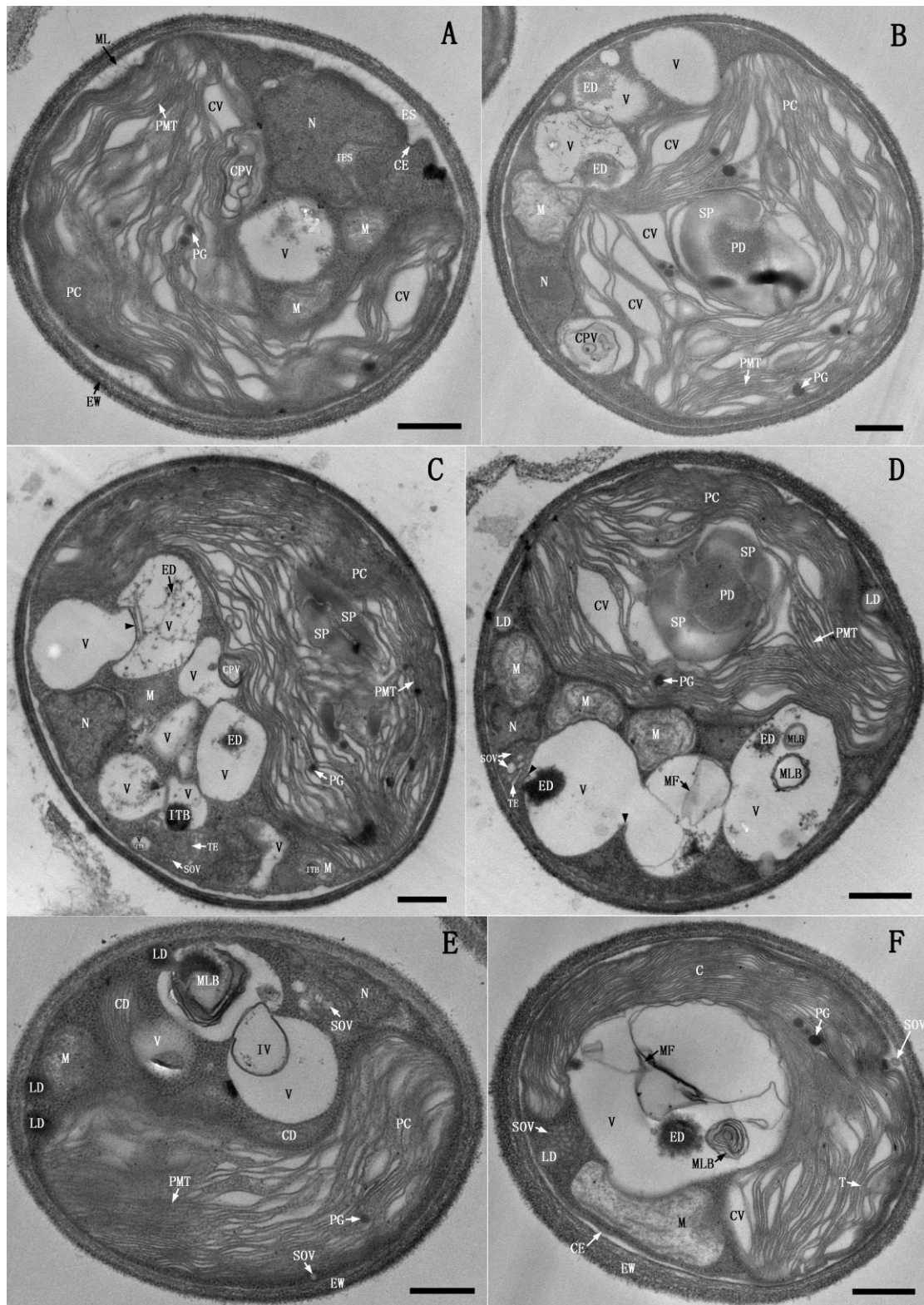


Figure 11. Formation and degradation of PMT-derived vesicles and coalescence of vacuoles. (A) A collection of short PMT 'rolled up' into "vesicle within vesicle" like compound vesicle (CPV) in PC margin. (B) A CPV was segregating from PC into EM. (C) A CPV was detaching from PC into a vacuole; while a large vacuole protruded into another one (arrowhead). (D) Membranes of the protruded vacuoles and the vacuole that contained membranous fragments (MF) fused at their contact site (arrowhead). (E) Two vacuoles were merging, in which a

LD was extruded from MLB; while a conspicuous piece of CD presented in EM. (F) PC got matured in chloroplast (C); all vacuoles coalesced into a single vacuole containing ED, MF and MLB. Scale bar, 0.5 μ m.

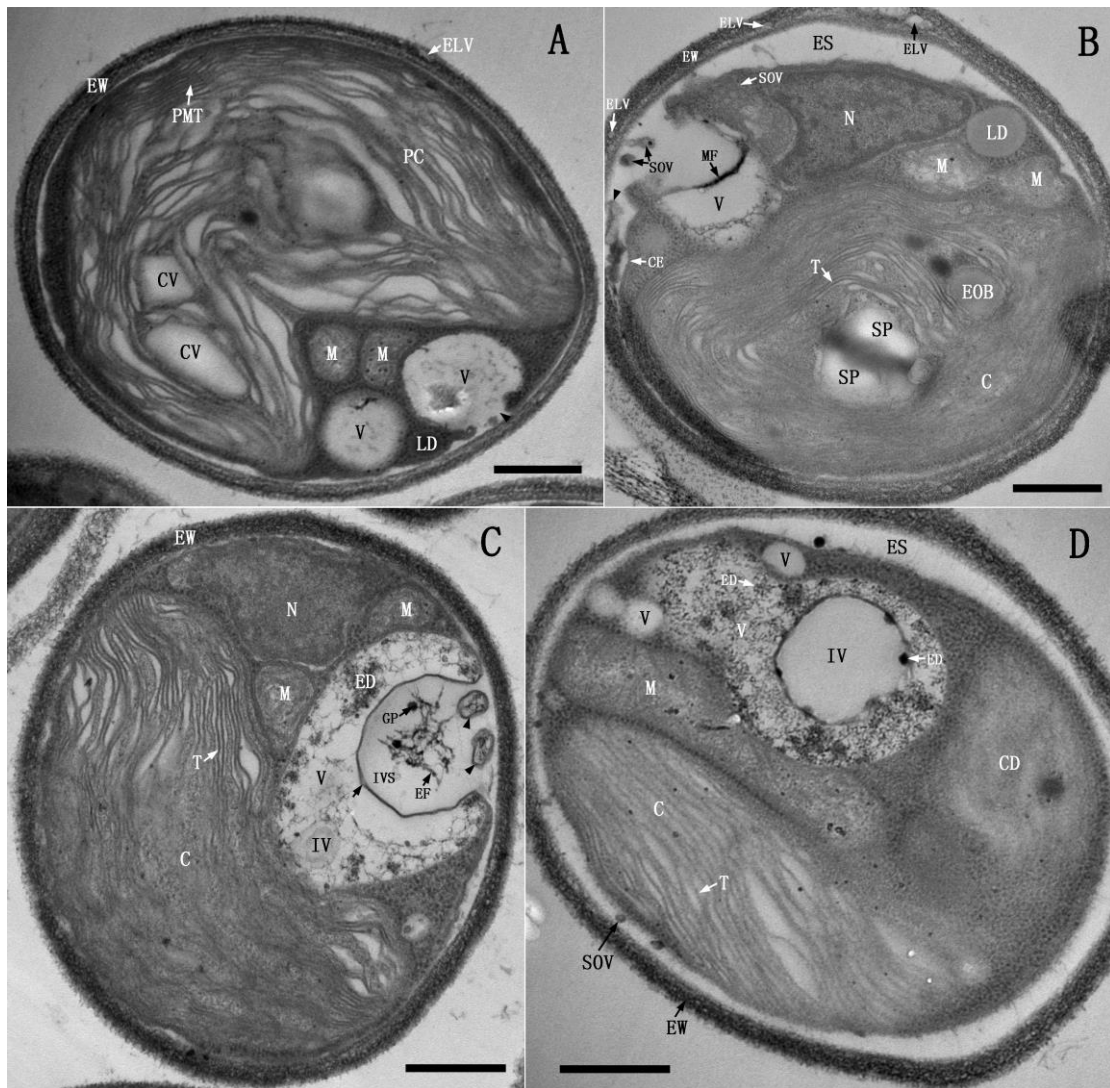


Figure 12. Vacuole mediated unconventional exocytosis and endocytosis. (A) An opening was formed at the contact site of the vacuolar membranes and CE (arrowhead), from which the vacuolar content was released. (B) The contacted vacuolar membranes and CE broke up into fragments (arrowhead), resulting in a wide opening, from which the soluble contents and SOV were expelled outside into ES. (C) The vacuolar membranes merged with the CE at two distant sites and then invaginated, resulting in a large invaginated space (IVS) entrapping some electron-dense fibrils (FB) and globular particles (GP); while CE between the two merged sites disrupted and coiled into membranous structures (arrowhead). It was clear that the invaginated vacuolar membranes consisted of two unit membranes (arrow). (D) A vacuole contained a large IV, which was in contact with a sausage-shaped mitochondrion and close to a CD. Scale bar, 0.5 μ m.

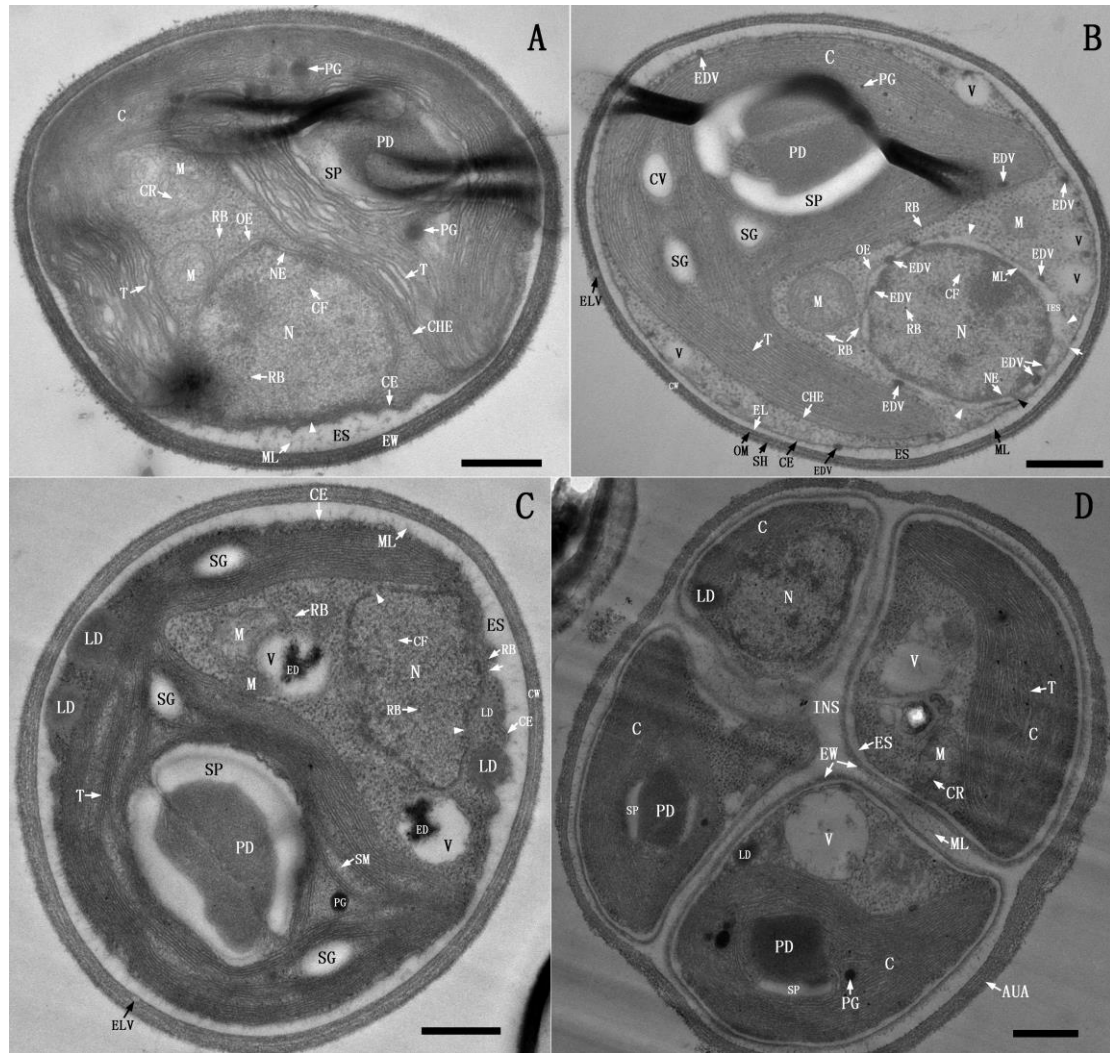


Figure 13. Structure and reproduction of TDX16-derived eukaryotic cell. (A) A TDX16-derived eukaryotic cell (TDX16-DE cell) contained an ‘e’-shaped chloroplast (C), a nucleus (N) and two mitochondria. The nucleus contained CF and some RB, whose OE and NE contacted and appressed to CE at the opening of chloroplast cavity (arrowhead). (B) Electron-dense vesicles (EDV) budded from NE (black arrowhead) into IES, and then fused with and re-budded from OE, ultimately reached the inner side of CHE and the two sides of CE. There were several openings at OE (white arrowhead), and one opening at the contact site of OE and CE (arrow). (C) OE and NE contacted intimately, on which large openings (arrowhead) were formed, and amazingly a fusion pore or conduit was formed at the contact site of NE, OE and CE (arrow). (D) Four developing autospores in an autosporangium (AUA) were segregated from each other by the wide interspace (INS). Scale bar, 0.5 μ m.

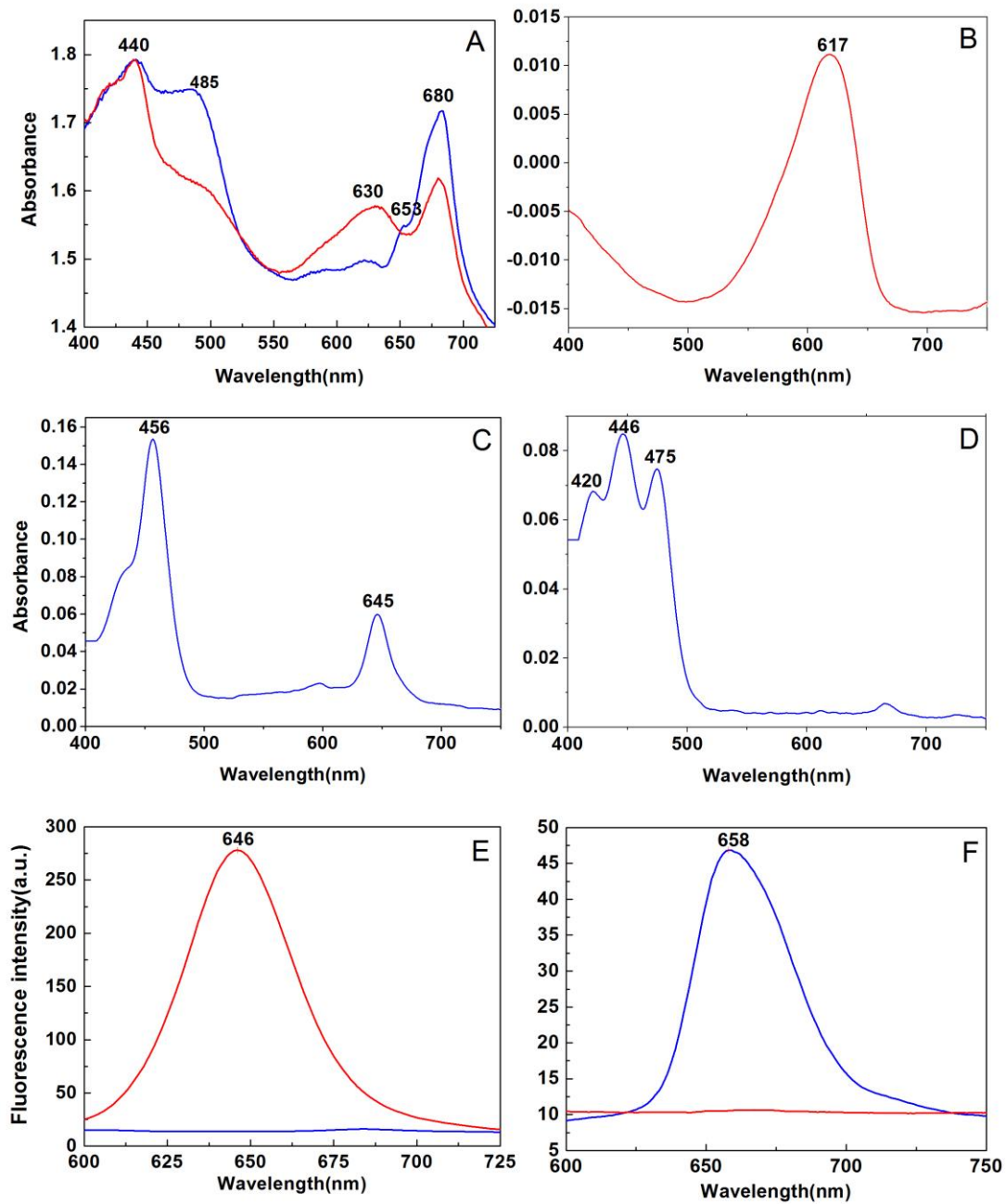


Figure 14. Absorption and fluorescence emission spectra. (A) In vivo absorption spectra of TDX16 (red) and TDX16-DE cell (blue). Absorption spectra of phycocyanin (PC) (B), chlorophyll b (C) and lutein (D). Fluorescence emission spectra of water soluble pigment extracts (E) and lipid soluble pigment extracts (F) of TDX16 (red) and TDX16-DE cell (blue).